A COMPUTATIONAL MODEL TO CHARACTERIZE DIFFERENT FLOW REGIMES FOR MICROSCALE RE-ENTRY SATELLITES

by

SUDHARSAN THIRUVENKADAM

Presented to the Faculty of the Graduate School of
The University of Texas at Arlington in Partial Fulfillment
of the Requirements
for the Degree of

MASTER OF SCIENCE IN AEROSPACE ENGINEERING

THE UNIVERSITY OF TEXAS AT ARLINGTON

December 2013

To my parents and relatives

who set the example and who made me who I am.

ACKNOWLEDGEMENTS

I would like to thank my supervising professor Dr. Harris Ben for his immense help during the course of my research work. He introduced me into the field of small satellites. It is his motivation and instructions that had pushed me to achieve the goals of the research work. I wish to thank Dr. Luca Massa and Dr. Brian Dennis for taking the time to serve in my thesis defense committee.

I would also like to thank my academic advisors Dr. Atilla Dogan, Dr. Wen chan, Dr. Albert Tong and all the teachers who have sharpened me towards achieving my goal. I would also like to thank Dr.Brian Dennis, Dr.Luca Massa and Dr. Luca Maddalena for introducing me into the field of computational fluid dynamics and coding environment. I would also like to extend my appreciation to Mrs. Debi Barton for her kindness in providing helpful information throughout my study at UTA. I am especially grateful to my other friends in satellite technology laboratory for their support and motivation.

Finally, I would like to express my deep gratitude to my sisters for encouraging me towards my goal. I am extremely grateful to my parents and relatives for their sacrifice, encouragement and patience. I would like to thank my friends Sridhar, Shanmuga Sundaram, Yogeswar, Aruna, Tee Cee, Anitha, Abisheik, Muruganandam and Dinesh Kumar for their support and guidance during hard phases of my life.

November 18, 2013

ABSTRACT

A COMPUTATIONAL MODEL TO CHARACTERIZE DIFFERENT FLOW REGIMES FOR MICROSCALE RE-ENTRY SATELLITES

SUDHARSAN THIRUVENKADAM, M.S.

The University of Texas at Arlington, 2013

Supervising Professor: Ben Harris

Atmospheric re-entry vehicles experience different flow regimes during flight due to the change in atmospheric density along the re-entry trajectory. This change in density creates non-equilibrium regions on the order of mean free path, called Knudsen layer. In the design of atmospheric re-entry vehicles, the flux variations near the wall of the re-entry vehicles are of critical importance. Traditional CFD simulations that use Navier-Stokes equations fail to predict the flow in the Knudsen layer. The Direct Simulation Monte Carlo (DSMC) method is accurate for all flow regimes, and correctly models the Knudsen layer but is computationally expensive. The computational cost increases as the number of molecules simulated increases. The areas where the rarefaction effects begin to dominate can be quantified by a Knudsen breakdown parameter (Kn). Traditional CFD can be improved with the use of slip boundary conditions in regions where the Knudsen breakdown parameter predicts the failure of continuum regime. In this thesis, a computational model has been developed to extend the validity of the continuum formulation with slip boundary conditions. The model uses the no-slip boundary conditions for continuum regime

($Kn < 0.01$), and Maxwell-Smoluchowski slip boundary conditions for slip regime ($Kn < 0.1$) in the free stream atmospheric properties. The results demonstrate the validity of the unified model in continuum and slip regime. For specific Knudsen number, flow predictions were validated against results from DSMC. The flow results matched within 10%.

TABLE OF CONTENTS

LIST OF ILLUSTRATIONS

LIST OF TABLES

CHAPTER 1

INTRODUCTION

1.1 Microscale Re-entry Satellites

A *satellite* is defined as a natural or artificial object in motion around a more massive body, where the motion is defined as an *orbit*, enabled by the dominant force of gravity from the massive body. When motion is dominated by gravity, the satellites trajectory can be modeled by a conic section, e.g. an ellipse. Recent advancements in the dynamics of extremely small satellites have their seeds in the behavior of dust particles in the solar system. These dust particles are very small so that the solar pressure and electrostatic forces cause them to have orbits that are not conic sections. Some of them find a stable orbit while others land like the space shuttle on the surface of a planet. At length and mass scales of the dust particles, the perturbing forces that are neglected in larger bodies can dominate the dynamics. This unique behavior motivates scientists and researchers to study the dynamics of extremely small bodies that can be harnessed and controlled to enable new space missions.

The concept of small artificial satellites has their seeds in the behavior of dust particles in the solar system. Based on the mass of the small artificial satellites, they are different types of small scale satellites. Microsatellites have a wet mass between 10 kg and 100 kg. The Swedish Space Corporation designed and developed two microsatellites. They are Astrid-1 and Astrid-2 [4, 5]. It carried two ultraviolet imager, one for imaging Earth's aurora and one for imaging alpha emissions from Earth's geocorona. With further advancement in electronics, development of nano sized satellites became popular among researchers.

Nanosatellites have a wet mass between 1 kg and 10 kg. Munin [6, 7] is a Swedish nano satellite developed by Swedish Institute of Space Physics (IRF) together with *Umeå* and *Luleå* Universities and Southwest Research Institute, San Antonio, Texas. The further advancement in satellite technology led to the design of picosatellites. Picosatellites have a wet mass between 0.1 kg and 1 kg. The CubeSats belong to the category of picosatellites. The CubeSats have a dimension of $10 \times 10 \times 10$ cm. The reference design of CubeSat was proposed by professors Jordi Puig Suari and Bob Twiggs [8]. Because of the lower production cost, a large number of educational institutions and companies around the world have developed CubeSats.

The advancement in satellite technology extended further with the design of femtosatellites with cost effective PCB approach [9, 10, 11]. The femtosatellite is an artificial satellite with mass between 10 g and 100 g. Several groups have been inspired by a variety of very small satellite concepts and supporting technology, including femtosatellites of mass less than 100 g. For example, Brown hosted a "Chipsat" workshop in 2010 [12]. The University of Michigan has explored the idea of using an electro-dynamic tether to provide propulsion for a satellite-on-a-chip mission [13]. Kicksat is a Cornell University effort funded by crowdsourcing [14].

1.1.1 Applications

There are several space and earth applications that can be supported with femtosatellite technology. *Remote sensing* is the acquisition of information about an object without making physical contact with it. The information is gathered by means of signals that are emitted or reflected from the object. The satellite-on-a-chip offers a reduced launch mass and distributed sensing opportunities, and it opens up a new research concept in space exploration. When thousands of microscale satellites are launched in space, they behave in a coordinated manner and provide

an unprecedented capability to investigate the widespread phenomena. A very good overview on this emerging technology can be found on Barnhart [10].

Space weather is the fluctuating environmental conditions in near-Earth space or the space between the Sun's atmosphere and a target planet atmosphere. It describes the changes in the ambient plasma, magnetic fields, radiation and other matters in space that are carried through interplanetary space by the solar wind from regions near the surface of the Sun. The microscale satellites, when launched in thousands into the orbit, could provide us with ample amount of information about the space weather. Each small satellite unit will telemeter the changes in plasma radiation and magnetic field variation to the Earth or to a main hub that gathers information from the distributed network of satellite systems. This network of scattered chips could produce 3D snapshots of space weather that no traditional spacecraft could do on its own.

1.2 Thermal Modeling

It is well known that all electronic equipment will be damaged if it is subjected to an extreme environment. A constraint for any space mission is to prevent overheating and undercooling of the satellite during all phases of the mission. The main source of the extreme temperature environment is the impact of atmospheric molecules on the spacecraft's wall to exchange their kinetic energy and momentum. The kinetic energy of the impacting molecules is in turn converted to thermal energy on the wall. This thermal energy plays an important role in proper functioning of the electronic components of the satellite. The goal of forming a distributed network of satellite-on-a-chip would be pointless unless a substantial number of satellites survive the extreme temperature environment of space. The survival rate of the satellite-on-

a-chip depends on several aerothermodynamic factors as boundary layer formation, Knudsen layer formation, and rarefaction effects.

Boundary layer is the layer of fluid that is formed in the immediate vicinity of a bounding surface where the effects of viscosity are significant. Most of the transport mechanisms occur within this layer. The thermal energy imparted by the impact of molecules is confined within the boundary layer. The boundary layer formation has to be analyzed carefully to understand the thermal environment around the satellite. More information regarding the boundary layer could be found in references [15]. The Knudsen layer is another layer that lies within the boundary layer of one mean free path in thickness. It is this layer that accounts for the rarefaction effects present locally in the flow.

A proper thermal model should account for the heat loss due to radiation and convection to the environment. There are several commercially available industry standard tools to carry out the behavior of near environment throughout the satellite trajectory. Some of them account for simulation in the rarefied atmosphere and some account for simulation in the continuum regime of the atmosphere.

1.3 Background Study

The above mentioned innovative concept of small satellites was successfully conveyed by a research group in Cornell. The Cornell research group developed a self-sustaining spacecraft demonstrating propellantless propulsion because of its small size. This self-sustaining spacecraft is called the "Sprite". Atchison et al. [16] used a aerothermodynamic model for numerically simulating the dynamics and aerothermodynamics of the "Sprite". This simple aerothermodynamic model was developed by Julian and Eggers [17] in 1957 for ballistic missiles entering Earth's atmosphere at hypersonic speeds. In this model, the body is assumed to be a single

thermal element free from radiation, gaseous imperfections and shock-boundary layer interaction. With the above mentioned assumptions, Julian and Eggers [17] carried out a simple aerothermodynamic analysis for predicting the maximum value of average heat transfer on the surface of the missiles.

Similarly, Koppenwallner et al. [18] studied the survivability of the screws and bolts of disintegrating spacecraft during re-entry, and proposed a fast analysis method with the following assumptions: flight dynamics [17], heating based on Stanton No., infinite heat conduction within the body, and averaged thermal data of materials. Despite several restrictions, the model Atchison et al. [16] adopted provided intuition about the thermal loading on the "Sprite". As the "Sprite" is very small in size, the single thermal element assumption could be a useful approximation for numerical simulations. This approximation fails to provide enough details about the thermal environment around these small-scale satellites. The design of small satellites require complete CFD analysis of the body and is the significant contribution of this thesis.

The CFD analysis of the body depends on the behavior of the fluid. The small-scale satellites are designed to enter into the planet's atmosphere with speeds governed by the re-entry dynamic equations. The atmospheric density variation causes the fluid around them to behave as a continuous medium or a rarefied medium. For motion through rarefied part of the atmosphere, the molecular structure of the air has to be taken into account. The impact of molecules on the surface of the re-entry body is responsible for the aerodynamic forces. In designing the CFD solver, the fluid behavior must be taken into account.

The critical atmospheric parameter for aerothermodynamic simulation is the density. It decreases exponentially with increase in altitude. This density decrease causes failure of the continuum formulation. Real gas flows are mainly viscous flows. To understand the flow behavior at different altitude, let us discuss a hypersonic

viscous flow over a flat plate in a full continuum atmosphere. When considering hypersonic speeds, the flow over a flat plate [1, 19] is divided into different regions as shown in Figure 1.1.

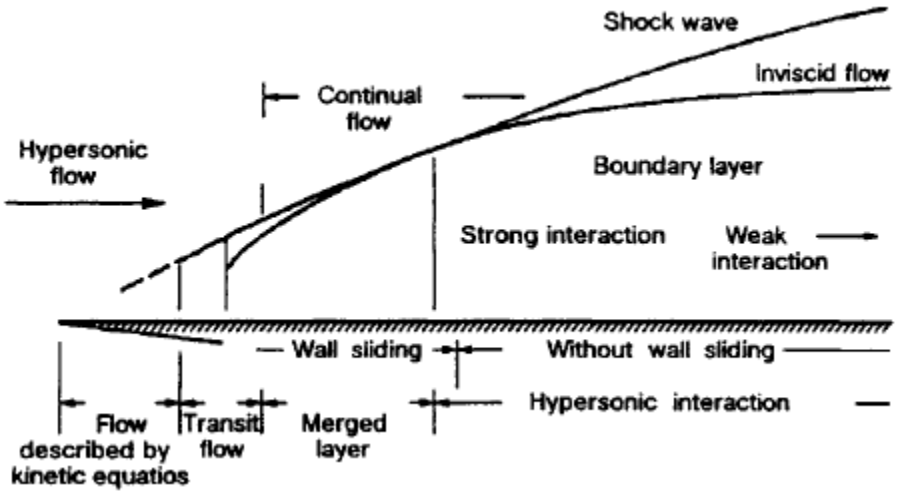

Figure 1.1. Hypersonic Flow over a Flat Plate [1].

In Figure 1.1, the region of flow immediately near the tip of the plate is rarefied. The flow in this region is governed by the kinetic theory. Immediately following the tip region, the shock and boundary layer merge to form a strong interaction region. In the strong interaction region, the flow behaves as a continuous medium, and the Navier-Stokes equations with no-slip boundary condition can be used to predict the flow properties. The shock wave and boundary layer interact and merge such that there is no inviscid zone in between them. Further downstream of the plate the shock layer coalesces into a discontinuity. This behavior develops a distinct inviscid layer between the shock and viscous layer. The effects of the rarefaction near the leading edge and the shock boundary layer interaction are studied by several researchers [20, 21].

In supersonic flow, the boundary layer and shock wave are far apart so that the interaction effects can be neglected [3].

Most of the hypersonic viscous flows exhibit the shock layer and boundary layer interaction. In most of the cases, the shock and boundary layer are assumed to have merged from the tip of the body. This assumption ignores the locally formed slip regime near the tip of the body. As a result, the equations derived using the continuum formulation can be utilized to develop the computational model for the merged shock-boundary layer. The boundary layer equations are the simplest set of governing equations. Even though the boundary layer equations are derived with continuum formulation it loses its validity for hypersonic flows. The locally formed rarefied region brings the slip effects within the viscous boundary layer. The solution procedure involves simultaneously solving the viscous and inviscid part together.

There exists another set of equations specifically designed for the merged shock and boundary layer assumption. This merged shock-boundary layer is the Viscous Shock Layer, and the equations governing this layer are called Viscous Shock Layer equations (VSL). The VSL equations are the modified version of the traditional boundary layer equations. The properties within this layer are similar to the thin boundary layer except with the x-direction pressure gradient (that is not zero because of the shock wave). The viscous shock layer equations have the advantage over the boundary layer equations in those regions where the shock wave and boundary layer interaction dominate. Thus, the interaction regions can be solved using the VSL equations through the marching approach [22, 23]. The main disadvantage of the VSL equations and boundary layer equations is its inability to account for the locally formed slip effects.

The disadvantage of the VSL and boundary layer equations can be removed by using the complete compressible Navier-Stokes equations. The continuum formulation

limits the use of Navier-Stokes equations. The viscosity of the fluid introduces the no-slip boundary condition at the fluid-wall interface. This no-slip boundary condition is at the center of fluid dynamic simulations until 1879. The local slip regime is one of the rarefaction effect that is found to exist in aerothermodynamic simulation. This part of the section discusses how the local slip regime is modeled in gas dynamics. The techique used to model local slip regime is used for extending the validity of Navier-Stokes equations for aerothermodynamic simulation.

In 1879, the possibility of gas slip was first introduced by Maxwell [24]. Maxwell described the existence of slip when the gas flow in devices with dimensions of the order of one mean free path. The mean free path is a kinetic parameter that states the average distance between the molecules. This slip condition is utilized for CFD simulations of microflows and nanoflows through channels whose dimensions are of one mean free path. Because of its relative simplicity, it is remembered as Maxwell's main theoretical result in rarefied gas dynamics. This Maxwell slip condition introduces the accommodation coefficient. The accommodation coefficient is defined as the fraction of heat or momentum transferred to the body. Maxwell's theoretical result has its limitation to flows over flat non-rotating surface by ignoring the normal velocity variation.

After the introduction of the slip condition, the continuum formulation of the Navier-Stokes equations are extended to predict the flows with local slip effects. Few authors have theoretically addressed the phenomenon of enhanced mass flow rates by employing the continuum equations in conjunctions with the application of Maxwell slip velocity. Following the conceptual paradigm of Maxwell slip, Arkilic et al. [25] employed a perturbation analysis of complete Navier-Stokes equations. However, the perturbation analysis and the slip condition constrained the model to be applicable for infinitesimally small values of Mach number and Reynolds number.

In 2005, Lockerby et al. [26] proposed a wall-function type for boundary in the Knudsen layer. This wall-function is another advancement in the continuum-fluid formulation. The viscosity is modeled as $\mu = \mu\psi^{-1}$. The ψ is derived by curve fitting the Knudsen layer velocity profile that was originally derived by Lockerby et al. [26] as:

$$\psi\left(n/\lambda\right) \approx 1 + \frac{7}{10}\left(1 + \left(n/\lambda\right)\right)$$

The use of the above formulation captures the Knudsen layer structure with the continuum-fluid formulation for locally non-equilibrium gas flows. This wall-function is based on the Boltzmann equation, and it improves the predictive capability of Navier-Stokes equations for a variety of flow configuration.

The behavior of the fluid particles is quantified by the scaling parameter. The scaling parameter, therefore, determines the governing equations required to solve the flow field. A brief introduction about the scaling parameters are explained in subsequent chapters of the report. Another different method that is used to solve for the rarefaction effects is the Direct Simulation Monte Carlo (DSMC). This method was proposed by Bird [2] and is based on statistics. Several research works compare the CFD results of flow with the experiment and Direct Simulation Monte Carlo Method for validation. Research works by Glass and Moss [27] focused on higher Knudsen number flows over a cylinder and sphere using the CFD, DSMC and collisionless DSMC for Earth entry conditions. Similarly another research from Brazil used the DSMC method for predicting the aerothermodynamics of Brazilian reusable satellite [28, 29]. He obtained the drag force, heat transfer coefficient and other aerothermodynamic characteristics for different Knudsen numbers ranging from the free molecular regime to the hydrodynamic (continuum) regime. The different regimes around the body are studied by varying the Reynolds number.

Greenshields and Reese [30] investigated the non-equilibrium (slip) boundary conditions with Navier-Stokes equations for rarefied hypersonic flow simulation over a flat plate with Patterson [31] and Smoluchowski temperature jump boundary conditions [32]. The jump boundary conditions are described in Section 3.5. The results indicate that the Patterson's jump condition compares quite well with DSMC and are consistently better than Smoluchowski jump condition. The better performance of the Patterson jump condition is the assumption on the flow being only slightly non-equilibrium. Most of this non-equilibrium effects originates because of the linear stress / strain relations in the continuum approach.

Lockerby et al. [33] reassessed the general first order slip boundary condition by implementing the full form of tangential stress. With this implementation of tangential stress, they proposed a new higher order model that has its validity extended to bodies having curvatures and rotational wall motion with the inclusion of thermal creep. Thermal creep is a phenomenon where the temperature gradient causes the slip from colder to hotter region. The results from this higher order model are compared with the DSMC results and analytical solution [34]. They also implemented the higher order boundary condition (Maxwell-Burnett boundary condition) to the Navier-Stokes equations instead of solving the complex nonlinear Burnett equations. This Maxwell-Burnett boundary condition is found to have reasonable agreement with the experimental values for Poiseuille flow.

Egorov and Erofeev [35] compared the continuum Navier-Stokes equations with slip/jump boundary condition of a flow past a flat plate with DSMC method. Egorov et al. used different types of slip boundary conditions for solving the Navier-Stokes equations with implicit finite-difference method. They proposed that the Navier-Stokes solution based on single Reynolds number does not depend on the characteristic length except for certain zone in the vicinity of the trailing edge.

All the above research works provide ample amount of information regarding the methods that should be used to develop a computational algorithm. The CFD simulation of hypersonic flows depends on the flow regime calculation that in turn depends on several parameters from the kinetic theory. This thesis focuses on the flow regime classification and CFD simulation of femtosats. The complete Navier-Stokes equations are used in this thesis because of the length scales of femtosats.

1.4 Objective of Thesis

Traditional CFD breaks down due to the rarefaction effects in the flow. The rarefaction effects are found to exist throughout the trajectory of the re-entry bodies. These rarefaction effects occur at different altitude depending upon the characteristic length of the body. The complex Boltzmann equation can be used to develop a unified computational model for predicting the flow properties throughout the trajectory, but this requires lot of computation resources. The Navier-Stokes equations require less computational resources than the Boltzmann equation. So a computational model based on Navier-Stokes equations is developed in this research work. The primary objective of this thesis is to develop an algorithm that predicts the flow behavior around small scale satellites at different altitudes. Furthermore, the model is applied to femtosats to show the possibility of surviving re-entry. This thesis ignores the locally formed slip effects and models the technique used for local slip effects for free stream slip conditions.

1.5 Outline of Thesis

The layout of this report is meant to guide the reader through the development of the thesis research. *Chapter 2* describes the aerothermodynamic effects, atmo-

spheric model and scaling parameters for flow regime classification which frames the initial part in the analysis. *Chapter 3* explains about the governing equations used for different flow regimes, numerical technique, discretization, stability of the numerical method and dsmcFOAM for free molecular simulation. *Chapter 4* talks about the simulation method, procedure followed in the analysis and free stream data points and discussion of the results. *Chapter 5* summarizes the results, contribution and future work.

CHAPTER 2

ATMOSPHERIC MODEL AND AEROTHERMODYNAMICS

2.1 Atmospheric Model

The aerothermodynamic simulation of re-entry bodies requires the free stream atmospheric properties as a function of altitude. The free stream atmospheric properties are the pressure (P_∞), temperature (T_∞), density (ρ_∞), and viscosity (μ_∞). The earth atmosphere consists of several layers, the troposphere at sea level to the thermosphere above 80 km. The free stream properties at every altitude depend on the constituents air molecules. The atmospheric model is a mathematical model constructed with the primitive equations governing the motion and behavior of air molecules [36]. The most important atmospheric parameter for aerothermodynamic simulation is density. The density variation determines the governing equations for computational simulation of aerothermodynamics.

Air is composed of several elements like Nitrogen (N_2), Oxygen (O_2), Argon (Ar) etc. These elements are present in different proportions at each altitude depending upon the temperature and pressure. The aerothermodynamic behavior of gas molecules near the surface of the body at re-entry speeds excites the internal energy of the molecules. As a result, the molecules dissociate and the solution procedure becomes complex. To avoid this high-temperature effects, the composition of the atmosphere can be considered as constant up to 100 km altitude for computational simulation of aerothermodynamics. The percentage of composition is merely an average number, and the composition of gas strongly depends on geographical latitude of a location.

2.2 Non-Dimensional Numbers

By knowing only the units of the parameters involved in a physical process, useful information can be deduced by grouping of similar parameters as dimensionless ratios. This technique is called *dimensional analysis*. It is a very powerful engineering tool. There are several dimensionless parameters involved in fluid dynamics simulation. The most critical dimensionless numbers used in fluid physics are the Reynolds number, Mach number and Prandtl number.

2.2.1 Reynolds Number

The Reynolds number is defined as the ratio of inertial forces to viscous forces in a flow. It is used to predict similar patterns in different fluid flow situations. It is also used to characterize different flow regimes within a similar fluid, such as laminar or turbulent flow. The laminar flow occurs at low Reynolds numbers, where viscous forces are dominant, and is characterized by smooth, constant fluid motion. The turbulent flow occurs at high Reynolds numbers and is dominated by inertial forces that tend to produce chaotic eddies, vortices and other flow instabilities. The Reynolds number is given by,

$$Re = \frac{VL}{\nu}$$

where V is the fluid velocity, L is the characteristic length and ν is the kinematic viscosity.

2.2.2 Mach Number

The Mach number is the ratio of vehicle velocity relative to sound velocity. Mach number varies by the composition of the surrounding medium and also by local conditions, especially temperature and pressure. The Mach number is used to

determine if the flow can be treated as incompressible or compressible. The Mach number is given by,

$$M = \frac{V}{c} \qquad c = \sqrt{\frac{\gamma k T_\infty}{m}}$$

where k is the Boltzmann constant, γ is the specific heat ratio, c is the sound velocity, γ is the specific heat constant and k is the thermal conductivity. The atmospheric temperature increases as a function of altitude. This increase in temperature in turn causes a decrease in Mach number. The sound velocity also varies from planet to planet. The Apollo Capsule entry conditions on Earth were 11 km/s (M=32.5, 53 km altitude), whereas the Galileo probe entered Jovian atmosphere at 60 km/s (M=28, 1000 km altitude). The Mach number was lower in the second case owing to the greater value of sound speed in the temperature of hydrogen-helium at that altitude.

2.2.3 Prandtl Number

The Prandtl number is the ratio of momentum diffusivity to thermal diffusivity. It is named after Ludwig Prandtl. It defines the stickiness behavior of the fluid. In viscous flows, the thermal and momentum boundary layer are the regions where most of the transport mechanisms occur. If the Prandtl number is higher, then the momentum boundary layer is bigger than the thermal boundary layer. If the Prandtl number is lower, the thermal boundary layer is bigger than the momentum boundary layer. The Prandtl number is given by,

$$Pr = \frac{\nu}{k}$$

where ν is kinematic viscosity and k is the thermal conductivity. For air the Prandtl number is 0.71.

2.3 Characteristics of Re-entry Flows

The characteristics of the re-entry flows fall into two kinds based on thermodynamic balance between properties: equilibrium and non-equilibrium. Consider any physical process that occurs due to the motion of air particles. The process could be anything that involves exchange of energy among various modes. The transfer of energy between the various energy modes is accomplished through molecular collisions or collisions between atoms and electrons with the surface. The time period of the molecules to stay on the surface is called the accommodation time, and it is determined by the frequency of the molecular collisions.

The equilibrium state is not found to exist at all the altitude because of the density variation. When the density is lowered, the non-equilibrium states are found to exist locally or throughout the domain. The non-equilibrium processes occur in a flow when the time required for a process to accommodate itself to the local conditions within a particular region is the same as the time taken by the air particles to cross that region. If the accommodation time is very short compared to the transit time, the process is in equilibrium. If the accommodation time is longer than the transit time, then the flow is frozen as it proceeds around the vehicle.

2.3.1 Equilibrium Flows

Equilibrium flows occur when the density is sufficiently high so that there are adequate collisions between particles to allow the thermodynamic balance between the molecules. For an equilibrium flow, any two thermodynamic properties can be used to define the state. As a result, the remaining properties and composition of gases can be determined.

2.3.2 Non-Equilibrium Flows

The non-equilibrium state occurs when the flow passes a strong shock wave (dissociation non-equilibrium) or undergo a rapid expansion (recombination non- equilibrium). In either state, there have not been sufficient collisions to achieve equilibrium during the fluid motion. If the rate at which the air particles move through the flow field is greater than the thermodynamic reaction rates, then the energy in the internal degrees of freedom is frozen within the gas. The non-equilibrium flow is found to exist at any altitude and at any flow velocity depending upon the rate of molecular collisions for energy transfer within them.

2.4 Aerothermodynamics

Aerothermodynamics is the study of thermodynamic state of the gases when travelling at very high velocities [37, 38, 39]. The thermodynamics of a moving fluid is characterized by the transport of 3 entities between molecules: the mass, momentum and energy. These entities are transferred between molecules through different mechanisms. Convective transport is a mechanism when a constituent part of the fluid entity is carried along with the fluid past a plane of unit area perpendicular to the velocity. This transport happens along the streamlines in a steady flow, and along pathlines in unsteady flow. If convective transport mechanism is dominant in a flow, then the flow is said to be inviscid.

Apart from the convective transport mechanism there are diffusive, turbulent and radiative transports. Diffusive transport is caused by non uniformities (gradients) in the flow field. The major phenomenon like viscosity, heat conduction and diffusion happens via the molecular transport of momentum, energy and mass respectively. If diffusive transport plays a major role, then it is called viscous flows. Turbulent

transport is due to fluctuations in turbulent flows. Radiative transport occurs due to the transfer of heat away from the surface due to radiation.

2.5 Aerothermodynamic Effects

The aerothermodynamic design process of any space vehicle is embedded with the vehicle design process. The aerothermodynamic design process includes the analysis of flow over a vehicle to estimate the thermal state of the surface and other surface effects. The atmosphere with its properties determines the free stream parameters of a flight vehicle. These in turn govern the aerothermodynamics and aerodynamic performance. As the upper atmosphere is highly rarefied, the spacecraft will not undergo any major thermal damage because the fluid behaves as individual molecules instead of continuum.

2.5.1 Thin Shock Layer

The shock layer is defined as the region that lies between the shock wave and the body surface. This phenomenon happens at hypersonic speeds where the density increase across the shock wave is directly proportional to Mach number. At hypersonic speeds, the distance between the shock and body is very small and the flow field between them is called as shock layer as described in Section 1.3. The thin shock layer is very critical at lower Reynolds number because of the boundary layer formation. At high Reynolds number, the flow field is inviscid.

2.5.2 Entropy layer

At hypersonic speeds, the entropy of the flow is directly proportional to the strength of the shock wave. The stronger the shock, the larger the entropy increase. This effect is common for hypersonic blunt vehicles. The strong entropy gradients

developed across the normal portion of the bow shock propagates downstream of the body. The boundary layer that is found to exist in any viscous flow lies within this entropy layer and is affected by it.

2.5.3 Viscous Interaction

The viscous behavior of the fluid causes the high velocity fluid particle to slow within the boundary layer. The loss in kinetic energy is transformed into internal energy of the gas (viscous dissipation). The increase in internal energy increases the temperature across the boundary layer and in turn the viscosity. As a result, the boundary layer becomes thicker. The major interaction between the boundary layer and the inviscid flow is called viscous interaction. It affects the surface pressure distribution and increases the skin friction and heat transfer.

2.5.4 High-Temperature Flows

The kinetic energy dissipated by a high speed gas due to skin friction can excite the vibrational energy of the molecules. Because of this excitation, the molecules are dissociated and ionized within the boundary layer. If the surface is protected with ablative material, this would result in chemical reaction in the boundary layer.

2.5.5 Low Density Flows

The density of the atmosphere varies as a function of altitude. As a result, the aerodynamic assumptions and governing equations tend to break down and fail to model the flow accurately. The altitude at corresponding to the continuum breakdown depends upon the characteristic dimensions of the spacecraft, and it can be found using the scaling parameter. For any space vehicle, the no-slip condition in the continuum zone fails, and there exists a slip in the fluid velocity near the wall (velocity

slip). Similarly, when the density is lowered, the gas temperature at the surface that is taken as wall temperature becomes something different (temperature jump). The traditional continuum assumption is valid with velocity slip and temperature jump conditions. All space vehicles have to pass through these aerothermodynamic effects in one way or the other.

The existence of local non-equilibrium gives rise to another layer similar to boundary layer called the Knudsen layer. The Knudsen layer is another aerothermodynamic effect that exists because of the density variation local to the body. The Knudsen layer is a very small layer and is of the order of one mean free path. It originates near the surface where the gas begins to exhibit non-equilibrium behavior. This non-equilibrium behavior is found to exist near the tip or nose of all hypersonic vehicles. In most CFD simulations, the small Knudsen layer emerging in a continuum regime is usually ignored.

2.6 Scaling Parameter

There are several notable parameters in kinetic theory. Among them, the number density and the mean free path are the vital parameters for defining the behavior of the flow. The ***Number density*** is defined as the number of molecules present in a volume. It is an intensive property. It is used to describe the degree of concentration in a physical space.. As an approximation, gas is considered as an aggregate of rapidly moving particles that are constantly colliding with each other. The influence of the particles on each other is significant when they are close enough so that the collision takes place.

The instantaneous velocity distribution and density distribution in gas particles are not uniform, and the statistical technique is often used to average the quantity instead of the instantaneous value. The coarseness of the structure of the gaseous

medium can be expressed the mean free path of the molecules. The ***Mean Free path*** λ is used as a qualitative characterization of the flow regimes, that we encounter in hypersonic flight. The approximate relation for mean free path is given by Vincenti and Kruger [40],

$$\lambda = (16/5)\frac{\mu}{\rho}\frac{1}{\sqrt{2\pi RT}} \tag{2.1}$$

The scaling parameter classifies the flow into different regimes: continuum, slip, transition and free molecular regime. The Boltzmann equation is valid in all regimes. The Navier-Stokes equations are valid in both continuum and slip regimes. The way these regimes are classified gives rise to different scaling parameters [41].

2.6.1 Tsein's Parameter

In 1934, Tsien [42] published an article on the aerodynamics of highly rarefied gases, a branch of fluid mechanics he called superaerodynamics. He proposed a parameter that is not based on the body dimension but on the boundary layer thickness. It is defined as the ratio of Mach number to the Reynolds number.

$$Kn = \frac{\lambda}{L} = \frac{M}{\sqrt{Re}}$$

2.6.2 Breakdown Parameter

The breakdown parameter is introduced by Bird [2]. This parameter classifies the flow regimes by accounting the density gradient in the flow direction. The breakdown parameter is given by,

$$P = \frac{1}{\nu}\left(\frac{D(\ln\rho)}{Dt}\right)$$

where ρ is the local density

2.6.3 Knudsen Number

The Knudsen number (Kn) is defined as the ratio of mean free path to the characteristic length of the body. The *overall* Knudsen number is a well known scaling parameter used to classify the flow regimes. The mean free path used in the kinetic theory is a state property and is defined in inertial frame of the gas. The following formulation for Knudsen number helps in understanding the flow rarefaction with information from free stream conditions.

$$Kn = \frac{\lambda}{L} = \left(\frac{\gamma\pi}{2}\right)^{0.5} \frac{M}{Re}$$

where λ is the mean free path, γ is the specific heat ratio. If M and Re are taken as the free stream conditions, then they account for free stream slip in the flow. If M and Re are taken as local conditions, then they account for local Knudsen layer formation. The Knudsen number is used as a scaling parameter in this thesis. Using the Knudsen number, the flow regimes are classified as continuum, slip, transition and free molecular regime.

Continuum: $Kn \leq .01$

Slip: $0.01 \leq Kn \leq .1$

Transition: $0.1 \leq Kn \leq 10$

Free Molecular: $Kn \geq 10$

CHAPTER 3

GOVERNING EQUATIONS AND NUMERICAL PROCEDURE

3.1 Overview of the Governing Equations

When developing an algorithm for problems governed by partial differential equations (PDE), selection of governing equations, numerics, stability and computational resources are to be taken into account. This section of the thesis report gives an overview of the available governing equations followed by a brief introduction of the Boltzmann equation and the traditional Navier-Stokes equations. Different scaling factors limit the use of governing equations for better prediction of flow properties in any hypersonic or supersonic flow simulation. The Knudsen number is used as the scaling parameter in this report, and its limits on the conventional formulation are shown schematically in Figure 3.1.

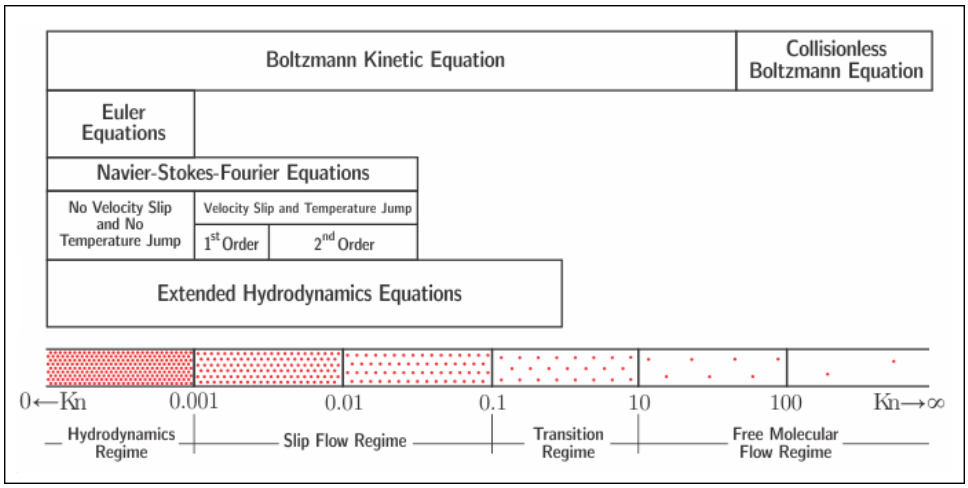

Figure 3.1. Knudsen Number Limits [2]..

The several set of partial differential equations used to design the computational model are as follows:

1. Boltzmann Equation [43]
2. Burnett Equations [44]
3. Full Navier-Stokes Equations
4. Reynolds Averaged Navier-Stokes Equations
5. Other Navier-Stokes Equations
   (a) Boundary layer equations
   (b) Viscous Shock Layer Equations [45]
   (c) Parabolized Navier-Stokes Equations
   (d) Thin Layer Navier-Stokes Equations

The evolution of the governing equations started with the statistical Boltzmann equation. It is reduced to the Burnett equations. The Burnett equation is further reduced to the Navier-Stokes equations. The Navier-Stokes equations are used in almost all kinds of fluid problems as long as the flow behaves like a continuum medium. As the Navier-Stokes equations requires a lot of computational resources, they are further reduced to Boundary layer equations.

Turbulence flows exhibit time dependent chaotic behavior. The Reynolds Averaged Navier-Stokes (RANS) equations are another form of Navier-Stokes equations that account for turbulence in the flow by adding the fluctuating properties. This inclusion of the fluctuating properties resulted in an extra term called Reynolds stress. When solving the Reynolds stress introduced in the RANS equations, Prandtl proposed the mixing length model that introduces a length scale called *mixing length*. The mixing length is defined as a distance that a fluid parcel will keep its original characteristics before dispersing them into the surrounding fluid. The mixing length is similar to the mean free path except that it defines the distance between two tur-

bulent clumps. Turbulent flows have different mixing length scales. The different mixing length scales of turbulent flows makes the numerical solution of the Navier-Stokes equations extremely difficult for turbulent flows.

There are two very significant advantages that would result when reduced equations are used instead of the full Navier-Stokes equations. First, there are fewer terms in the equations that reduce the computation time. Second, the reduced equations are parabolic in the streamwise direction and the same solution methodology as the boundary layer type equations can be used. Though the reduced equations require some additional methods to solve the entire flow domain, they are still a useful kind of equations to predict the flow behavior with less computational effort than the full Navier-Stokes equations.

3.2 Mathematical Behavior of Governing Equations

The governing equations that define the physics of the flow are non-linear partial differential equations. The solution vector of a PDE depends on several factors. The mathematical behavior of the governing equations reflects different physical behavior of the flow fields. There are several methods to find the mathematical behavior of the governing partial differential equations. All these methods rely on finding the characteristic lines along which certain properties remain constant. In simple, these characteristic lines are the directions along which information is transmitted in physical problems governed by PDE. Equations that exhibit wave-like solutions are known as hyperbolic. Equations whose solutions cor- respond to damped waves are known as parabolic. Finally, if the solutions are not wave-like, then the equations are designated as elliptic.

3.2.1 Hyperbolic Equation

The hyperbolic equations consist of two real characteristic lines. In Figure 3.2, the two characteristic lines intersect at point P. If we set up a disturbance at point P, then this disturbance is felt everywhere in the region I between the two characteristic lines. Now extending the two characteristic lines to the boundary, the solution at P is obtained just by marching forward in x. This shows that the solution at P depends on the boundary and that region is called as domain of dependence of a point P. Thus, the algorithm to solve hyperbolic PDE is set up as marching solutions with the given initial conditions (say y axis) and sequentially calculate the flow field step by step by marching in a specific direction.

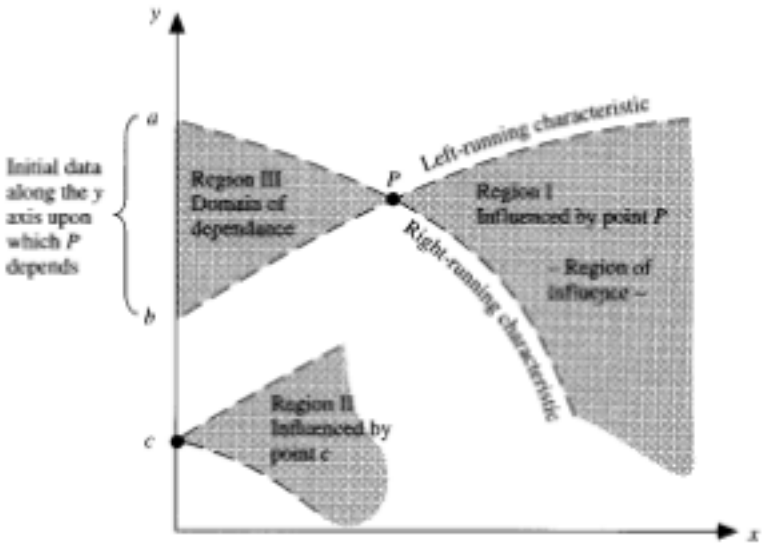

Figure 3.2. Hyperbolic PDE Behavior [3]..

3.2.2 Parabolic Equation

The parabolic equations have only one characteristic line between two boundaries. In the following Figure 3.3, the initial data is fed to the dark shaded line “ac”,

and the characteristic line passes through the point "P". Now any disturbance at point "P" is fed to the shaded region. Like hyperbolic equations, the solution for parabolic equations can be obtained through marching method.

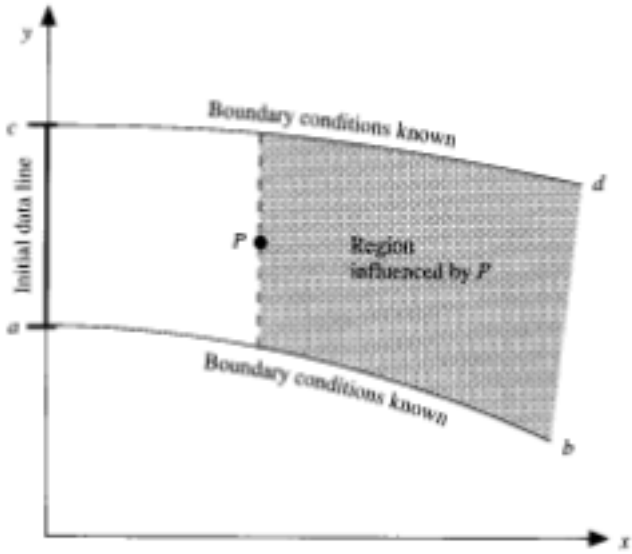

Figure 3.3. Parabolic PDE Behavior [3]..

3.2.3 Elliptic Equation

The elliptic equations have imaginary characteristic lines that make the method of characteristics useless for the solution of elliptic PDE. In Figure 3.4, the disturbance induced at P is propagated in all directions. Thus, the solution procedure for elliptic PDE is carried out by simultaneously solving all other nodal points in the domain.

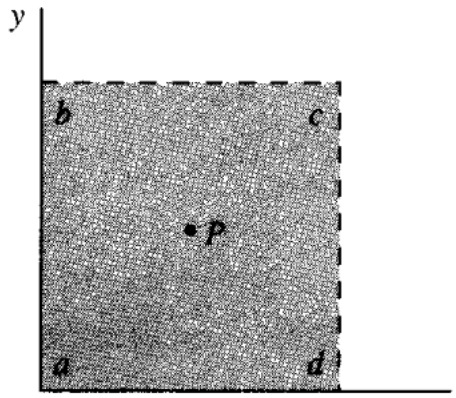

Figure 3.4. Elliptic PDE Behavior [3]..

3.3 Boltzmann Equation

The fundamental equations governing the fluid flow at the particle level is the Boltzmann equation [43]. It was devised by Boltzmann in 1872. It describes the non-equilibrium system behavior statistically. The Boltzmann equation is derived by assuming that all the molecules are identical sphere of equal radius. Let us assume a gas medium of unit volume, and it contains 10^{20} (Avagadro number) of molecules moving in a very irregular pattern. Each molecule is identified by its position and velocity vector in three dimensions.

$$\dot{x}_i = V_i \qquad \dot{v}_i = X_i \tag{3.1}$$

where X_i is the force acting on each individual molecules and i=1, 2, N. A *phase space* is a mathematical space in which all possible states of a system can be represented. The above representation of 3 position vectors and 3 velocity vectors can be represented in phase space (6N dimensional space) to reduce the complexity of the equation.

Before describing the terms in the Boltzmann equation, it is necessary to understand the Liouville equation. The Liouville equation is a fundamental equation of

statistical mechanics, and it provides the complete description of a system both in equilibrium and non-equilibrium state. The Liouville equation states that the density or mass of the system is conserved in the process. This forms the basis for the derivation of the continuity equation macroscopically. Now let us assume a probability density function $P_N(z,t)$ of the system of N-particles described earlier. This introduction of the probability density function satisfies the definition of Liouville Equation, and it is represented as,

$$\frac{\partial P_N}{\partial t} + \nabla \cdot (P_N Z) = 0 \tag{3.2}$$

Taking molecular collisions into consideration, the integration of the Eq. 3.2 results in a nonlinear complex integral term on the right hand side. The solution to the Boltzmann equation lies in the difficulty of collision integral. When replacing the probability density function by means of distribution function *f*, we have the famous Boltzmann equation given by,

$$\frac{\partial f}{\partial t} + v \cdot \frac{\partial f}{\partial x} = f(x,v,t) \tag{3.3}$$

The function *f(x,v,t)* on the right hand side of the Eq. 3.3 is called the distribution function, and a major achievement of classical kinetic theory is the development of Chapman-Enskog theory for the coefficients of viscosity, heat conduction and diffusion. The Chapan-Enskog method assumes the distribution function as a small perturbation from the equilibrium state, Maxwellian function f_0. It frames the base from which the Navier-Stokes equations, Euler Equations, and higher order Burnett equations are derived. The Chapman-Enskog distribution function is given by,

$$f = f_0(1 + aKn + bKn^2) \tag{3.4}$$

where the constants are function of gas density,temperature and macroscopic velocity vector and f_0 equilibrium Maxwellian distribution function.

The zeroth order solution of Eq. 3.4 where the viscous stress tensor and heat flux vectors vanishes corresponds to the Euler equations. It is valid in all regimes with exclusion of viscous effects. The first order expansion of Eq. 3.4 results in the Navier-Stokes equations. It represents a first order departure from the thermal equilibrium. The second order expansion of Eq. 3.4 results in Burnett equations. The Burnett equations yield accurate results than the Navier-Stokes equations because of its higher order accuracy. Higher order approximations of the Chapman-Enskog function yields the "Super Burnett Equations". The Super Burnett Equations have the highly nonlinear Burnett stress and heat transfer terms. This heat transfer and nonlinear Burnett stress terms are enormously challenging in both computationally and in terms of understanding the physics.

In general, the local fluid flow is classified into continuum, slip and free molecular regime. The Boltzmann Equation is valid throughout all the three regimes as it is a molecule based model. More information regarding the rarefied gas can be found in Kogan [46] and Bird [2]. Now the recent advancement is the use of Maxwell first order slip boundary conditions with the Navier-Stokes equations.

The determined distribution function has a three dimensional velocity space. Even for a two dimensional case, the number of nodal points for the distribution function is of the order of millions. Thus, the numerical solution of Boltzmann equation requires a large amount of computing resources and the solution of kinetic equation becomes intensive with increase in the number of nodal points. Also, the process of stabilization of the solution is very slow with increase in the number of nodes. There are several research works that focus on the numerical solution of the Boltzmann equation [47, 48].

3.4 Navier-Stokes Equations

The traditional CFD involves numerical simulation of the Navier-Stokes equations assuming the continuum formulation throughout the body. The Navier-Stokes equations are the first order approximation to the Chapman-Enskog function. The Navier-Stokes equations can also be obtained by applying the Newton's law to the fluid motion. The Navier-Stokes equations are nonlinear partial differential equations that are used in all problems as long as the continuum assumption is valid. The nonlinearity of the PDE makes the problem difficult to account for the turbulence that occur in the flow. Attempts to solve turbulent flows using a laminar solver results in convergence failure. Now ignoring the small slip regime that originate near the tip of the flat plate, full unsteady compressible Navier-Stokes equations [3] is given as follows:

Continuity:

$$\frac{\partial \rho}{\partial t} + \frac{\partial (\rho u)}{\partial x} + \frac{\partial (\rho v)}{\partial y} = 0 \tag{3.5}$$

x-Momentum:

$$\frac{\partial (\rho u)}{\partial t} + \frac{\partial}{\partial x}(\rho u^2 + P - \tau_{xx}) + \frac{\partial}{\partial y}(\rho uv - \tau_{yx}) = 0 \tag{3.6}$$

y-Momentum:

$$\frac{\partial (\rho v)}{\partial t} + \frac{\partial}{\partial x}(\rho uv - \tau_{xy}) + \frac{\partial}{\partial y}(\rho v^2 + P - \tau_{yy}) = 0 \tag{3.7}$$

Energy:

$$\frac{\partial E_t}{\partial t} + \frac{\partial}{\partial x}((E_t + P)u + q_x - u\tau_{xx} - v\tau_{xy}) + \frac{\partial}{\partial y}((E_t + P)v + q_y - u\tau_{yx} - v\tau_{yy}) = 0 \tag{3.8}$$

In the above equation, E_t is physically the sum of kinetic energy and internal energy per unit volume e which is defined as,

$$E_t = \rho \left(e + \frac{V^2}{2} \right)$$

The shear and normal stress are expressed as gradient of velocity which is given as below:

$$\tau_{xy} = \tau_{yx} = \mu \left(\frac{\partial u}{\partial y} + \frac{\partial v}{\partial x} \right)$$

$$\tau_{xx} = \left(\frac{2\mu}{3} \right) (\nabla \cdot V) + 2\mu \frac{\partial u}{\partial x}$$

$$\tau_{yy} = \left(\frac{2\mu}{3} \right) (\nabla \cdot V) + 2\mu \frac{\partial v}{\partial y}$$

The components of heat flux vector are given as:

$$q_x = (-k) \left(\frac{\partial T}{\partial x} \right)$$

$$q_y = (-k) \left(\frac{\partial T}{\partial y} \right)$$

There are nine unknowns embedded in the equations that cause closure problem and to close the equations, additional five equations are needed as described below:

$$P = \rho RT \qquad e = c_v T \qquad |V| = \sqrt{u^2 + v^2} \qquad Pr = \frac{\mu c_p}{k}$$

The viscosity is given by Sutherland's Viscosity law, which is as follows:

$$\mu = \mu_0 \left(\frac{T}{T_0} \right)^{1.5} \frac{T_0 + 110}{T + 110} \tag{3.9}$$

3.5 Boundary Conditions

The boundary conditions play a major role in defining the surface properties of any body in CFD simulation and are the actual driver for any CFD simulation. The number of boundary conditions and initial conditions depend upon the highest order of the derivative terms in space and time dimension. The Navier-Stokes equations have derivatives of second order of the velocity components u and v in both axes. Hence we have to prescribe two boundary conditions in both axes for each velocity component. One pair of the boundary conditions is defined at the body surface and

the other for external flow. It has a first order time derivative. So, an initial condition of the properties have to be specified.

3.5.1 No-Slip

The boundary condition on any surface in viscous flows assumes zero relative velocity between the surface and the gas immediately next to the surface. This condition is called no-slip boundary condition. The no-slip condition gives rise to the boundary layer that incorporates all the wall interaction phenomena. Along with this is the temperature boundary condition that states the fluid temperature immediately next to the wall has the same temperature as the wall. The no-slip and constant wall temperature constraints imposed by the viscous flows are given by,

$$u = v = w = 0 \tag{3.10}$$

$$T = T_w \tag{3.11}$$

3.5.2 Maxwell Slip

The Knudsen layer accounts for the local rarefaction effects at low Knudsen number. The Boltzmann equation has to be solved in the Knudsen layer with a specified molecular reflections at the wall. Recently several at- tempts have been made to establish the slip conditions without solving the Boltzmann equation. With the introduction of Maxwell slip boundary condition, the validity of the Navier-Stokes equations is found to extend till slip regime.

The Maxwell slip-Smoulouski jump boundary conditions [33] are the first order slip and jump boundary conditions used to predict the slip effects originating on the surface. It is given by,

$$u_s - u_w = \left(\frac{2-\sigma}{\sigma}\right)\lambda\frac{\partial u_x}{\partial n} + \frac{3\mu}{4\rho T}\frac{\partial T}{\partial x} \tag{3.12}$$

$$T_s - T_w = \left(\frac{2-\alpha}{\alpha}\right)\lambda\frac{\partial T}{\partial n} \tag{3.13}$$

where the first term in Eq. 3.12 is the slip introduced due to velocity gradients and the second term is due to the wall transpiration. The constants σ and α are known as the velocity and thermal slip coefficients respectively. They are also known as tangential momentum and energy accommodation coefficients. These constants are purely dependent on the surface properties and are determined experimentally.

The accommodation coefficients describe the gas-wall interactions and requires complete knowledge of the scattering kernels. The thermal accommodation coefficient is based on the energy fluxes of the incident and reflected molecules. The tangential momentum accommodation coefficient is based on the momentum of the incident and reflected molecules. The values of these slip coefficients define the wall reaction to the incident fluid particles/molecules. The wall reactions are commonly classified as specular and diffusive reflection. The case of $\sigma = 0$ is called specular reflection. In this case, there is no tangential momentum exchange of fluid with the wall, resulting in zero skin friction. This is the limit of inviscid flow, where the viscous stresses are zero.

$$\frac{\partial u_s}{\partial n} \longrightarrow 0$$

The case of $\sigma = 1$ is called diffusive reflection where the molecules are reflected from the wall with zero average tangential velocity. This is an important case of tangential momentum exchange and friction of gas with the walls. There are several

higher order slip models proposed and validated that makes it easier to account for the local non-equilibrium region with the continuum formulation [49]. The validity of the governing equations with the above mentioned slip and no-slip conditions are tabulated in Table 3.1

Table 3.1. Flow Regimes and Models

Flow Regime	**Knudsen No.**	**Fluid Model**
Continuum	$Kn \leq .01$	Navier Stokes Eq with no slip B.C
Slip	$0.01 \leq Kn \leq .02$	Navier Stokes Eq with slip B.C
Slip	$0.02 \leq Kn \leq .1$	Burnett Eq with Slip B.C
Transition	$0.1 \leq Kn \leq 10$	Burnett Eq with Slip B.C DSMC Lattice Boltzmann
Free Molecular	$Kn \geq 10$	Collisionless Boltzmann DSMC Lattice Boltzmann

3.6 Numerical Analysis

Analytical solutions of partial differential equations involve closed form expressions that give the variation of dependent variables throughout the domain. Problems that governed by nonlinearity require numerical methods to obtain the solution numerically. In numerical analysis, the domain is broken down into discrete points by the process of discretization, a process by which continuous models and equations are transferred into discrete counterparts. The governing equations are written in discrete form called the difference equation. The difference equation is solved at each and every grid points, and the solution vector is obtained.

When solving the discretized algebraic equations at the grid points, the following criteria should be taken into consideration:

1. The discretization of PDE must become exact as the step size tends to zero (consistency).
2. Numerical errors that arise because of step size should not be amplified.
3. Numerical solution should converge to the exact solution as the step size tends to zero.

All the above criteria should be taken into account for successful numerical algorithm. This section describes about the errors that are found to exist in numerical simulation and the type of numerical method used in designing the computational model. The conservation form of the above mentioned compressible Navier-Stokes equations is given in Eq. 3.14.

$$\frac{\partial U}{\partial t} + \frac{\partial E}{\partial x} + \frac{\partial F}{\partial y} = 0 \tag{3.14}$$

where the matrices U, E and F are given as follows:

$$U = \begin{bmatrix} \rho \\ \rho u \\ \rho v \\ E_t \end{bmatrix}$$

$$E = \begin{bmatrix} \rho u \\ \rho u^2 + P - \tau_{xx} \\ \rho uv - \tau_{xy} \\ (E_t + P)u + q_x - u\tau_{xx} - v\tau_{xy} \end{bmatrix}$$

$$F = \begin{bmatrix} \rho v \\ \rho uv - \tau_{xy} \\ \rho v^2 + P - \tau_{yy} \\ (E_t + P)v + q_y - u\tau_{xy} - v\tau_{yy} \end{bmatrix}$$

When the above conservation form is written with the time derivative on the left hand side and the rest of the terms on the right hand side of the equation, then the approach is said to be the *time-dependent approach*. The time marching solution is obtained by solving the dependent variables progressively in steps of time. When the solution vector is solved, it results in numerical values for the products ρu, ρv, ρw, E_t . These products are called *flux variables*. The primitive variables are ρ, u, v, w, e are extracted from these flux variables through Eq. 3.15–Eq. 3.19.

$$\rho = \rho \tag{3.15}$$

$$u = \frac{\rho u}{\rho} \tag{3.16}$$

$$v = \frac{\rho v}{\rho} \tag{3.17}$$

$$w = \frac{\rho w}{\rho} \tag{3.18}$$

$$e = \frac{\rho(e + V^2/2)}{\rho} - \frac{u^2 + v^2 + w^2}{2} \tag{3.19}$$

3.6.1 MacCormack Method

The Numerical technique used in the simulation is the well known MacCormack technique [50]. It is an explicit time dependent method slightly different from the two-step Lax-Wendroff scheme [51]. Both methods are used for governing equations that exhibit parabolic and hyperbolic mathematical behavior. The *unsteady* Navier-Stokes equations have mixed parabolic and elliptic behavior, and that makes the MacCormack technique suitable method for the Navier-Stokes equations. In solving the *unsteady* Navier-Stokes Equations, the time derivatives are written on the left side, and spatial derivatives are written on the right side of the equations. The overall numerical procedure is contained in two step: the Predictor and Corrector step. The spatial derivatives are replaced by forward and rearward differences in

predictor and corrector steps respectively.

Predictor Step: In this step, the solution vector for the next time step is guessed by using forward differences.

$$U_{i,j}^{t+\Delta t} = U_{i,j}^{t} + \left(\frac{\partial U}{\partial t}\right)_{av} \Delta t \tag{3.20}$$

The derivative is calculated using forward differences from the known flow field variables at time t+1 by,

$$\left(\frac{\partial U}{\partial t}\right)_{i,j}^{t} = -\frac{E_{i+1,j}^{t} - E_{i,j}^{t}}{\Delta x} - \frac{F_{i,j+1}^{t} - F_{i,j}^{t}}{\Delta y} \tag{3.21}$$

The predicted values of the flow field variables are obtained as follows:

$$\bar{U}_{i,j}^{t+\Delta t} = U_{i,j}^{t} + \left(\frac{\partial U}{\partial t}\right)_{i,j}^{t} \Delta t \tag{3.22}$$

Corrector Step: In correction mode, the initially guessed values for the solution vector are corrected using backward differences.

$$\left(\frac{\partial \bar{U}}{\partial t}\right)_{i,j}^{t+\Delta t} = -\frac{\bar{E}_{i,j}^{t+\Delta t} - \bar{E}_{i-1,j}^{t+\Delta t}}{\Delta x} - \frac{\bar{F}_{i,j}^{t+\Delta t} - \bar{F}_{i,j-1}^{t+\Delta t}}{\Delta y} \tag{3.23}$$

The average of the above two derivatives at time t and t+Δt are substituted in Eq. 3.20 to obtain the solution vector at time t+Δt.

3.7 Stability Analysis of the Numerical Method

There is a link between the characteristic curves and the step size of the marching variable that elucidates the physical significance of the stability. This connection is explained with the numerical domain and analytical domain of the solution vector. The numerical domain is the region between the characteristic lines where the solution is obtained at all grid points by marching in a specific direction. The analytical domain is the region where the actual solution is found to exist for the problem. For stability, the numerical domain must include all the analytical domain.

3.7.1 Errors

Numerical analysis of any physical problem is an approximate way to obtain the solution. Because it is an approximate method, errors do exist normally in the numerical analysis. The way that these errors are propagated from one step to another step in the marching direction determines the stability of the numerical method. These errors must be kept within limits or else it gets amplified every time step and make the numerical method go unstable. It can be minimized when the step size in marching direction is imposed with certain criteria for which the numerical solution remains unaffected. The limit of the marching variable can be obtained by carrying out a stability analysis of the finite difference form.

There are different sources of errors that influence the numerical solution of a governing differential equation. *Discretization error* is the difference between exact solution of difference equation and exact analytical solution of the partial differential equation. *Round-off error* is the numerical error which is introduced into the solution after a repetitive number of calculations in computer that constantly rounds off the solution to significant figure. *Truncation error* is the error made by truncating the infinite sum and approximating it to finite sum.

3.7.2 Stability Criteria

When carrying out a numerical simulation, it is necessary to analyze the stability of the numerical method. The stability criteria for compressible flow is given by MacCormack [52],

$$(\triangle t_{CFL})_{i,j} = \left[\frac{|u_{i,j}|}{\delta x} + \frac{|v_{i,j}|}{\delta y} + a_{i,j}\sqrt{\left(\frac{1}{\delta x^2} + \frac{1}{\delta y^2}\right)} + 2\acute{v}_{i,j}\left(\frac{1}{\delta x^2} + \frac{1}{\delta y^2}\right)\right]^{-1} \tag{3.24}$$

where

$$\acute{v}_{i,j} = max\left[\frac{(4/3)\mu_{i,j}(\gamma\mu_{i,j}/Pr)}{\rho_{i,j}}\right]$$

The stability criteria of time step imposes the following value for the stability of the solution.

$$\triangle t = min[K(\triangle t_{CFL})_{i,j}]$$

where K is the fudge factor that accelerates the solution based on its value. The value of K ranges from 0.3 to 0.6.

3.8 Software

There are many commercially available CFD simulation softwares to carry out the thermal modeling of satellites. Among all the tools, the Rarefied Aerodynamic Modeling System for Earth Satellites (RAMSES), and Spacecraft Atmospheric Reentry and Aerothermal Break up (SCARAB) [53, 54, 55] provides advantages in modeling rarefied regimes. These tools provide a user interface so that we can model the spacecraft dynamics and CFD together. Apart from these commercially licensed softwares, there exists an open source toolbox for development of customized numerical solvers and pre-/post processing utilities for several CFD problems called OpenFOAM.

OpenFOAM [56] is an open source CFD tool available for Unix-based environment. It consists of several CFD solvers that can be modified based on the problem. This section of the report gives information about the rarefied gas analysis solver incorporated within OpenFOAM by Scanlon et al. [57]. The main purpose of this solver is to perform steady and transient solutions for any arbitrary 2D/3D geometries.

3.8.1 dsmcFOAM

Bird [2] introduced the DSMC method to simulate rarefied gases. The DSMC method is a statistical method to solve equations governing real gases. In this method,

a real gas is modeled as millions of simulated molecules for computational efficiency. The fundamental principle behind DSMC method is splitting of continuous collisions of molecules and its motion inside the domain at each time step $\triangle t$ into two sequential stages namely the collision relaxation and free-molecular transfer.

As the molecules move, they collide with other molecules and with boundaries. The locations and velocities of each of the simulated molecules is determined and stored after every time step. The major aspect of DSMC method is each simulated molecules corresponds to millions of real molecules. All the real molecules represented by single simulated molecules are assumed to share the same mass, position coordinates and velocity. It reduces the calculation effort. The deterministic molecular motion and the probabilistic molecular collision are uncoupled using a computational time step that is smaller than the mean collision time. Both time discretization and space discretization are important in DSMC simulation.

As the DSMC method is based on statistics, it may subject to significant statistical errors or fluctuations. Several research works showed that this error is proportional to the square root of the number of particles used in the simulation. Thus, an ideal DSMC simulation should contain a sufficient number of particles to faithfully represent a sample size in order to reduce this potentially significant error. This serves as a successful method to predict the macroscopic properties of flows in free molecular regime. Bird's DSMC procedure consists of the following steps :

1. Select number of simulated molecules.
2. Calculate the time step.
3. Break down the domain into several cells just like traditional CFD but with limitations imposed on the cell size.
4. Index the molecules in each cells and each cells into subcells.
5. Track the molecules.

6. Select collision pairs.
7. Calculate post collision properties.
8. Sample the macroscopic flow properties.

The above mentioned procedure is implemented in OpenFOAM as dsmcFOAM. DsmcFoam is an open source solver that is used to numerically simulate low density regimes through statistical approach. It has been well known tool for many years in solving molecular dynamics [58]. This method although suitable for almost all kinds of flow regimes, it finds its vast usage for higher Knudsen numbers and for higher Mach numbers. This method, however, becomes a poor simulation tool for low speed flows about the micro devices because huge sample size is required to reduce its inherent statistical errors.

CHAPTER 4

SIMULATION AND RESULTS

4.1 Computational Model

The free stream atmospheric properties define the rarefaction effects on the surface of re-entry bodies. Re-entry satellites start their journey at high hypersonic speeds and descend to subsonic speeds before it reaches the planet's surface. Throughout their journey, there are different regimes build up around them depending on its speed and the free stream atmospheric properties. These flow regimes are responsible for the near environment property change around the satellites.

At higher altitudes, the satellite experience the impact of molecules on their surface and this defines the aerothermodynamic properties around the satellites. This is because at higher altitudes the atmosphere is highly rarefied (the density is very low) and the molecules are widely separated from each other. At lower altitudes (below 80 km), the atmospheric molecules are closely packed, and the impact is felt as the collection of molecules (volume) instead of a single molecule. The intermolecular distance is responsible for the free stream rarefaction effects. The rarefaction effects define the breakdown of the governing partial differential equations.

In this thesis, a computational algorithm is developed to model the continuum and slip flow regimes for femtosat length scales. The computational algorithm is designed and validated for a flat plate of length 1×10^{-5} m and 1 cm. The free stream atmospheric properties are the primary inputs to any commercially available CFD tool as it serves as the input boundary condition to the partial differential equations. These free stream atmospheric conditions are defined by the U.S. Standard

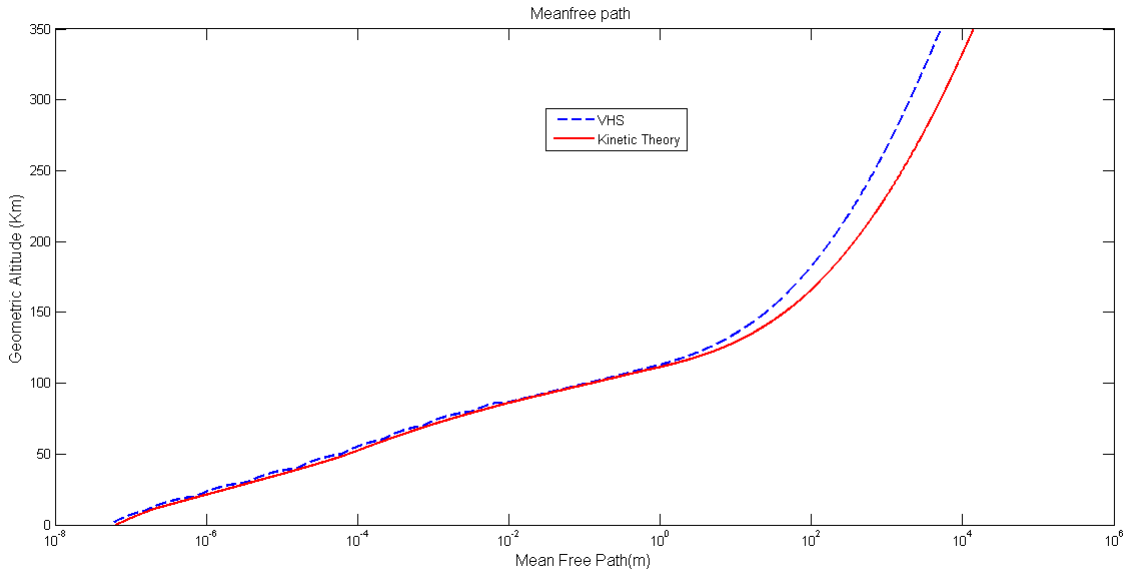

Figure 4.1. Variation of Mean free path.

Atmosphere 1976 [36]. The experimental data for the mean free path below 80 km is obtained from Bertin [39] and Hirschel [37]. It is then added to the Standard Atmosphere code.

The mean free path is obtained with two different formulations: one with kinetic theory and the other with Eq. 2.1. The mean free path obtained via Eq. 2.1 and with the kinetic theory is given in Figure 4.1.

Figure 4.1 shows that there is not much variation in the mean free path predicted by the two theories, but there is a significant deviation from those predicted by kinetic theory at higher altitude and the data predicted by Eq. 2.1. The mean free path is an important parameter in designing the computational model, and it is a vital function for the breakdown parameter. For classifying the free stream atmospheric properties, the mean free path predicted by kinetic theory is used.

The rarefaction effects are then found and modeled using the Knudsen breakdown parameter. The Knudsen breakdown parameter is calculated at every altitude

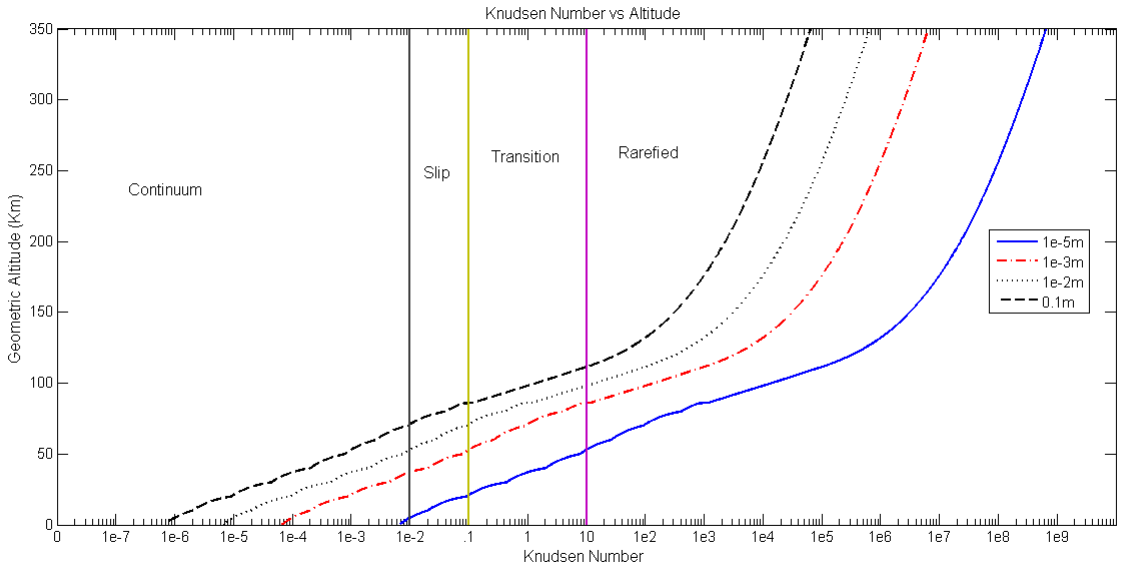

Figure 4.2. Variation of Knudsen number.

for the characteristic length of the re-entry satellite. The small-scale satellite is modeled as flat plate to validate the computational model. Figure 4.2 concludes the flow regime characterization for different characteristic length of the flat plate.

The above plot shows the occurance of different flow regimes at different altitude for different characteristic length of the satellite. Another important parameter that should be taken into consideration is the dynamic viscosity μ. The dynamic viscosity is modeled using two laws: Sutherland viscosity law and Power law approximation. The Sutherland viscosity is given by Eq. 3.9, and the Power law is given by,

$$\mu = \mu_{ref} \left(\frac{T}{T_{ref}} \right)^{\omega} \tag{4.1}$$

where the reference viscosity is given by Variable Hard Sphere theory (VHS) [2], T is the translational temperature and ω is the VHS temperature exponent (viscosity index). The power law approximation is used to model dynamic viscosity for dilute gases. The dynamic viscosity of pure nitrogen or any of the gas constituents can be

Table 4.1. Molecular Properties of N_2

m	4.65×10^{-26} kg
d_{ref}	4.17×10^{-10} m
T_{ref}	273 K
μ_{ref}	1.656×10^{-5} pa-s
ω	0.74

modeled using the Power law. The gas is assumed to be composed of Nitrogen (N_2), and the molecular properties of Nitrogen are given in Table 4.1. This assumption is made for flow simulation and validation in slip regimes.

After the flow regimes are characterized, the governing compressible Navier-Stokes equations (Eq. 3.4–Eq. 3.4) are written in the general form (Eq. 3.14). The MacCormack technique is then used to discretize the solution vector (U). After the predictor and corrector step, the flow variables are extracted from the flux variables through Eq. 3.15–Eq. 3.19. The no-slip and slip boundary conditions are used accordingly for regions that fall in the continuum and slip regimes respectively. The boundary conditions are applied throughout the wall surface ignoring the locally formed different flow regimes.

The computational model is purely developed with the equations governing the fluid motion and its behavior. To analyze the flow behavior of the small-scale re-entry satellites along its trajectory path, the re-entry dynamics equations are to be solved along with the fluid equations at every time step. This must be done to input the exact Mach number and the corresponding free stream properties at that altitude. For testing the computational algorithm, the results are obtained for an assumed supersonic and hypersonic Mach numbers.

4.2 CFD Simulation Parameters

The major input parameters are the free stream atmospheric properties (pressure, temperature, density and velocity). The results for different speeds and different altitudes are discussed in subsequent sections. The characteristic length is chosen to be 1×10^{-5} m, as the validity of continuum regime extends inversely with the characteristic length.

Table 4.2. Free Stream Conditions

Alt (Km)	**P** (Pa)	**T** (K)	**Density**(kg/m^3)	**No. Density**	**Kn**
Sea	101325	1.218	288.16	2.4799×10^{25}	0.005
1	8.9876×10^4	1.1116	281.6612	2.3146×10^{25}	0.00559
2	7.9501×10^4	1.0065	275.1725	2.1493×10^{25}	0.006
3	7.0121×10^4	0.9092	268.6837	1.9839×10^{25}	0.00653
4	6.1660×10^4	0.8193	262.1950	1.8186×10^{25}	0.007
5	5.1048×10^4	0.7363	255.7062	1.6533×10^{25}	0.007833
6	4.7218×10^4	0.6600	249.2175	1.4879×10^{25}	0.009
7	4.1105×10^4	0.5899	242.7287	1.3226×10^{25}	0.00979
8	3.5652×10^4	0.5257	236.24	1.1573×10^{25}	0.0112
9	3.0801×10^4	0.4670	229.7512	9.919×10^{24}	0.01306
10	2.65×10^4	0.4135	223.2625	8.266×10^{24}	0.0156
11	2.27×10^4	0.3648	216.65	7.6184×10^{24}	0.017
12	1.9399×10^4	0.3119	216.65	6.9706×10^{24}	0.0186
13	1.6580×10^4	0.2666	216.65	6.3229×10^{24}	0.02048
14	1.417×10^4	0.2279	216.65	5.6752×10^{24}	0.02282
15	1.2112×10^4	0.1948	216.65	5.0275×10^{24}	0.02576
50	79.8737	270.65	0.010	2.0851×10^{22}	0.0056
51.8	63.87	269.6131	8.2427×10^{-4}	1.8162×10^{22}	0.0071
54	48.3987	263.5708	6.3970×10^{-4}	1.4964×10^{22}	0.009
60	21.9584	247.0643	3.1001×10^{-4}	6.1887×10^{21}	0.02

From Table 4.2, the plate length of 1×10^{-5} m experiences continuum regime till 7 km, and the computational model uses no-slip boundary conditions to predict the flow parameters. Beyond that altitude there occurs the breakdown in the continuum

assumption, and the computational model uses slip boundary conditions to predict the flow parameters till 15 km where the Knudsen number is 0.02.

The free stream atmospheric properties that are used to test the computational model are tabulated in Table 4.2. The domain is basically a rectangular in shape with the flat plate boundary defined at the bottom. Table 4.3 and Table 4.4 gives the domain information for L=1 $\times$ 10^{-5} m and L=1 cm respectively.

Table 4.3. CFD Input Conditions for L=1 $\times$ 10^{-5} m

Mach no.	4 &15
$\triangle$x	1.4493×10^{-7}
$\triangle$y	1.1869×10^{-7}
No. of Cells	3600, 4900, 6400
Altitude	sealevel - 7 km (Continuum) 8 km - 22 km (Slip)

Table 4.4. CFD Input Conditions for L= 1 cm

Mach no.	4
$\triangle$x	1.4493×10^{-4}
$\triangle$y	1.2841×10^{-4}
No. of Cells	4900
Altitude	sealevel - 55 km (Continuum) 56 - 75 km (Slip)

4.3 DSMC Simulation Parameters

In this method, the actual number of real molecules are represented by equivalent number of particles. The time and space discretization are important for the DSMC simulation. For time discretization, the DSMC particles move during every

time step and then they collide with each other after every time step. For space discretization, the flow field is divided into cells, and they serve for two purposes: Selection of collision pairs and to obtain macroscopic properties in every cell.

The input free stream parameters to the dsmcFOAM are tabulated in Table 4.5.

Table 4.5. DSMC Input Parameters

No. Density	**No. of DSMC particles**	**Kn**
2.4799×10^{20}	3×10^{12}	0.005
8.3023×10^{19}	1.4×10^{12}	0.0156
2.9150×10^{19}	3.84×10^{11}	0.04
1.7934×10^{19}	3×10^{11}	0.072
1.0372×10^{19}	2×10^{11}	0.124
1.3012×10^{18}	2.60×10^{10}	0.9952
1.9291×10^{17}	3.858×10^{9}	6.713

There are two different kinds of errors in DSMC simulation: statistical errors and deterministic errors. The statistical error is introduced due to the stochastic nature of the method. The deterministic error is due to the scaling in both time and space discretization. Several research works are carried out to improve the accuracy of the DSMC method. All those research works concluded that the cell size should be no greater than 1/3 in the gradient direction. The following conditions [2, 59] are to be followed when using DSMC method.

1. The flow field should be discretized such that the ratio of the cell dimension to the mean free path is less than 1/3%.

$$\frac{\triangle x}{\lambda} = \frac{\triangle y}{\lambda} \leq 1/3 \tag{4.2}$$

2. The time step chosen should be such that it is 1/3 of the mean collision time. The mean collision time is the time taken by the particle to cover a distance of one mean free path with the most probable speed c_0.

$$\frac{\triangle t}{\lambda / c_0} \leq 1/3 \qquad c_0 = \sqrt{\frac{2kT}{m}} \tag{4.3}$$

The computational domain for the DSMC simulation is given in Table 4.6. The domain for DSMC simulation should be modeled in such a way that it satisfies Eq 4.2 and Eq. 4.3.

Table 4.6. DSMC Domain

Mach no.	4
$\triangle$x	3.46×10^{-5}
$\triangle$y	3.44×10^{-4}
Plate Length	1 cm
No. of Cells	50750

4.4 Results and Discussions

The computational model is tested with two different characteristic lengths of the flat plate: 1×10^{-5} m and 1 cm. For the plate length of 1×10^{-5} m, the no-slip and slip boundary conditions are tested, and the results are plotted for different Knudsen numbers. To test the computational model developed in this thesis, two different Mach numbers are used as the input parameters. The result section is subdivided into two categories: continuum regime results and slip regime results.

4.4.1 Continuum Regime Results

This section discusses the results predicted by the computational model in the continuum regime. The computational model uses the traditional no-slip boundary conditions for the flow prediction. The trajectory points are selected such that the flow regime is within continuum regime.

Kn=0.005

At a Knudsen number of 0.005, the flow is within the continuum regime (No-slip regime). Even though the flow is in continuum regime, there is an evidence of continuum breakdown near the tip of the plate due to the formation of shock at supersonic and hypersonic speeds.

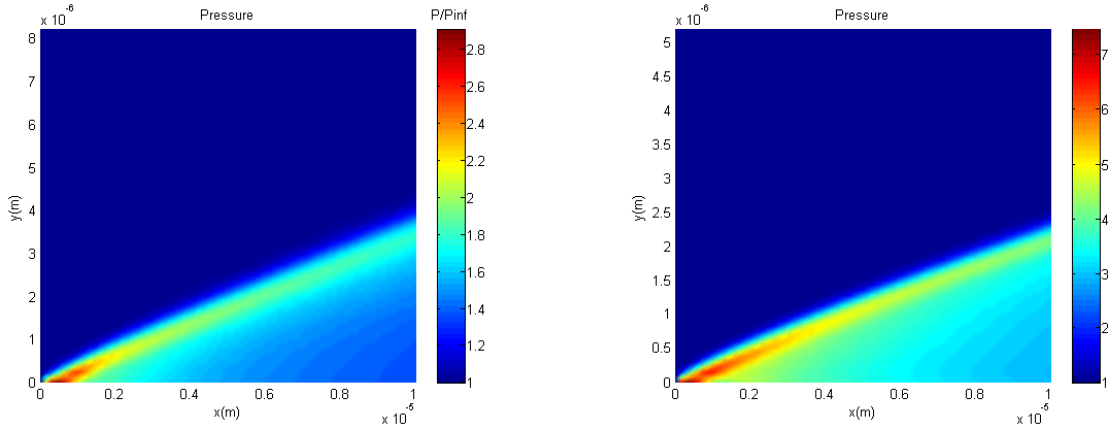

(a) (b)

Figure 4.3. Pressure Contours for Kn=0.005 (a) Mach 4, (b) Mach 10.

When investigating the density of two different flows, there is a lesser amount of rarefaction in hypersonic flows than the supersonic flow because of the distance between the shock and the plate wall. In Figure 4.3, we see the pressure build up on the surface increases with increase in the strength of the shock wave.

The temperature contour in Figure 4.4 for M=10 shows an increase in the magnitude of 2.5 times than the M=4 because of the several aerothermodynamic effects that are dominant in hypersonic flows. The breakdown is well understood from the density contour (Figure 4.5) along the surface. The density increases across the shock wave.

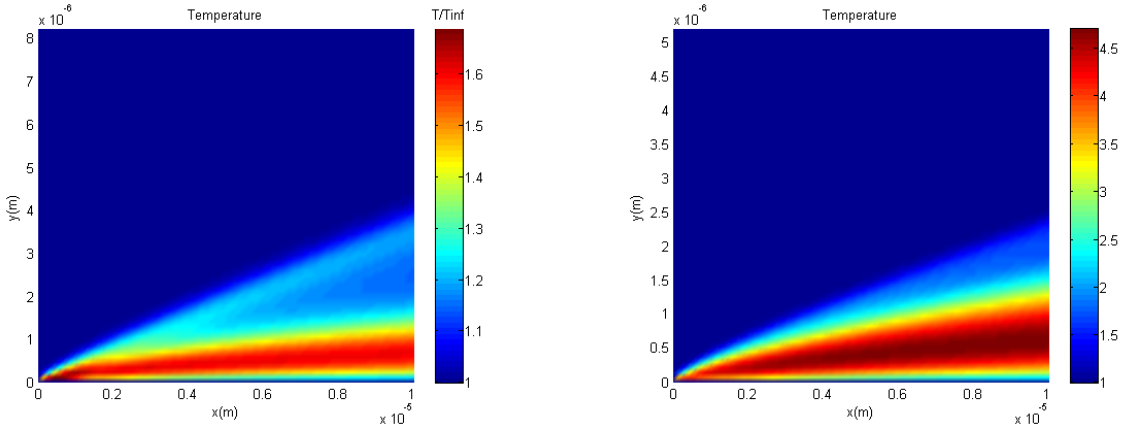

(a) (b)

Figure 4.4. Temperature Contours for Kn=0.005 (a) Mach 4, (b) Mach 10.

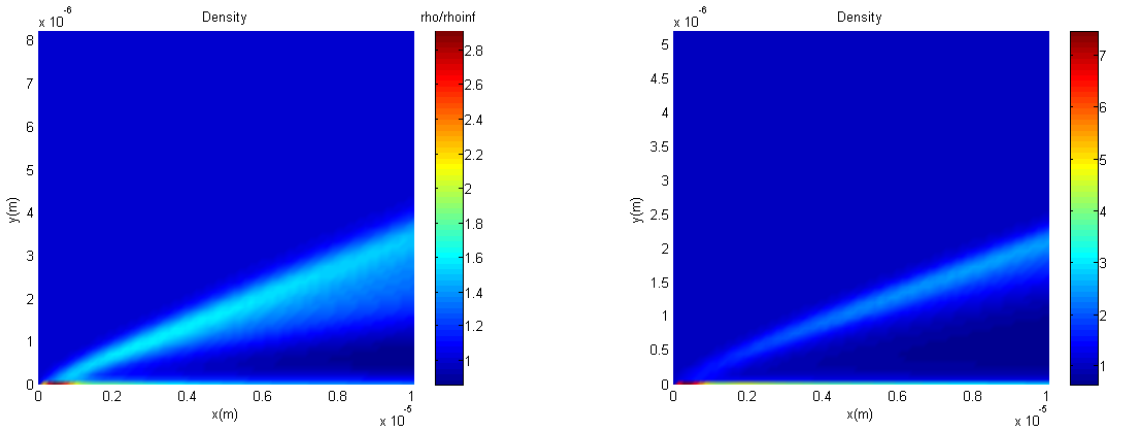

(a) (b)

Figure 4.5. Density Contours for Kn=0.005 (a) Mach 4, (b) Mach 10.

Kn=0.007

At Kn=0.007, the flow is still in continuum regime.

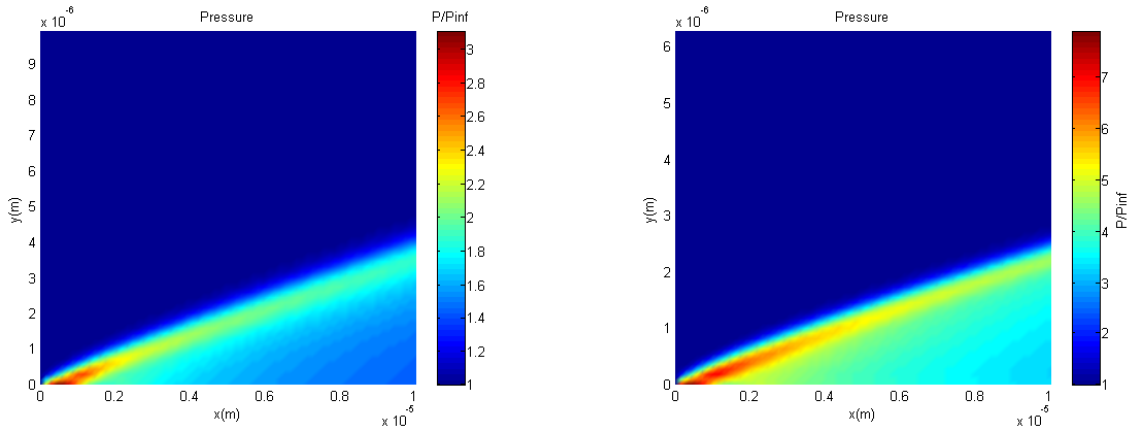

(a) (b)

Figure 4.6. Pressure Contours for Kn=0.007 (a) Mach 4, (b) Mach 10.

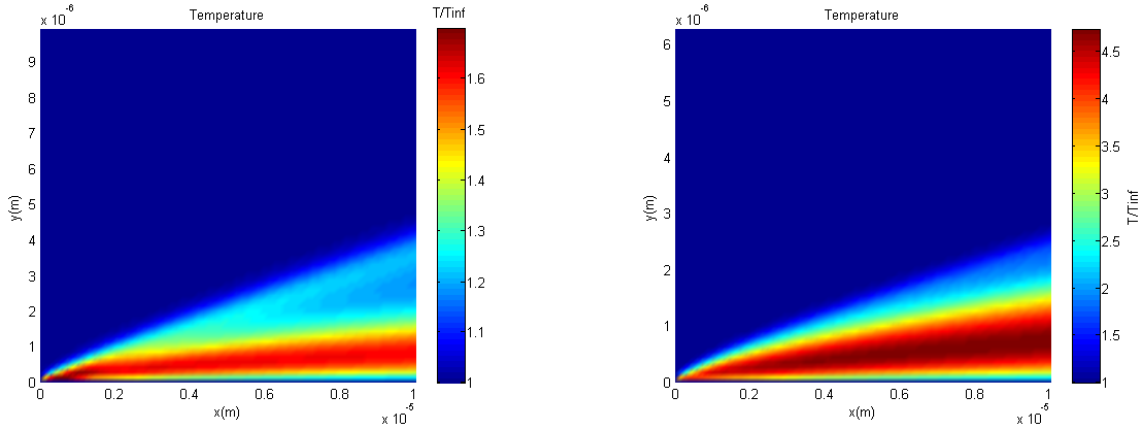

(a) (b)

Figure 4.7. Temperature Contours for Kn=0.007 (a) Mach 4, (b) Mach 10.

Figure 4.6 shows the variation of pressure at M=4 and M=10. The pressure increase in this flow regime is 2 times stronger than the M=4 case. This pressure

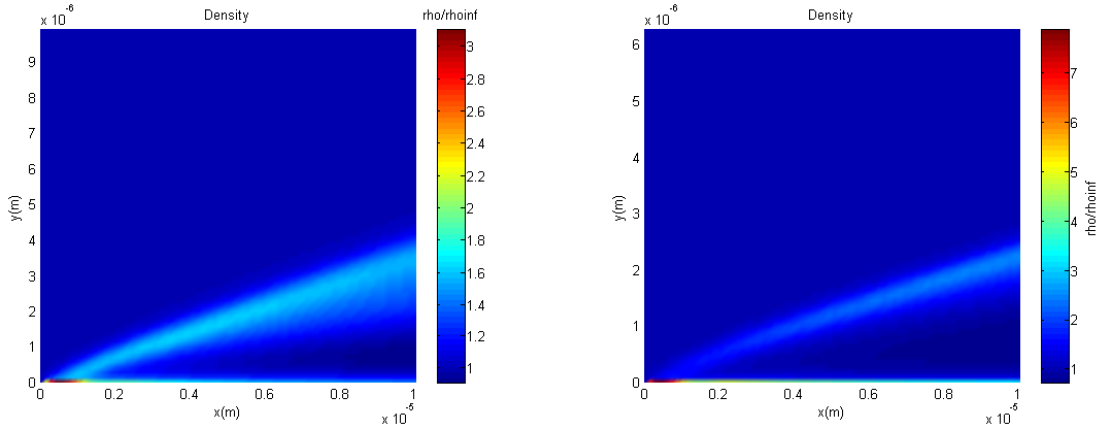

(a) (b)

Figure 4.8. Density Contours for Kn=0.007 (a) Mach 4, (b) Mach 10.

increase is lower because of the decrease in free stream pressure conditions. Figure 4.7 shows the temperature variation for different Mach numbers. Figure 4.8 shows the density contour for M=4 and M=10.

Kn=0.009

At Kn=0.009, the flow is considered to be near the limit of continuum regime.

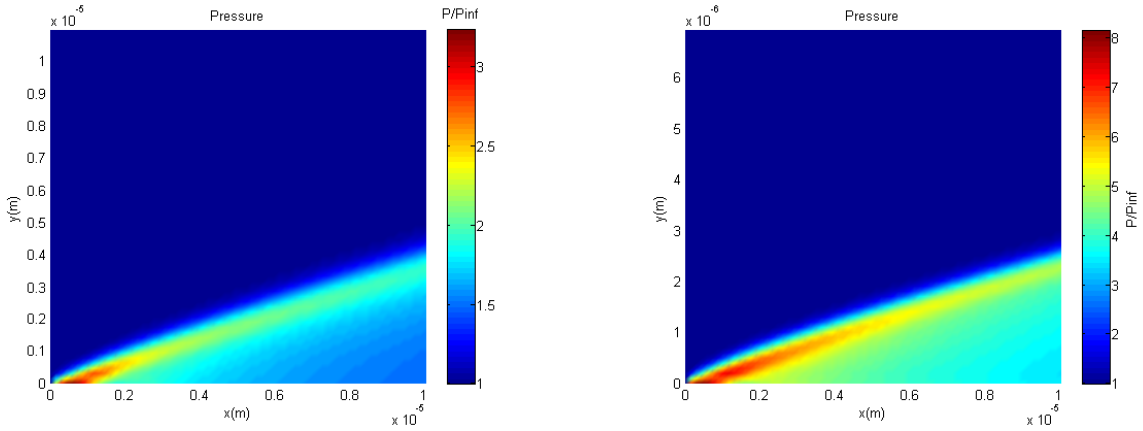

(a) (b)

Figure 4.9. Pressure Contours for Kn=0.009 (a) Mach 4, (b) Mach 10.

Figure 4.9 and Figure 4.10 shows the pressure and temperature variation for different Mach numbers. The increased evidence of the breakdown can be figured out from the density contour in Figure 4.11.

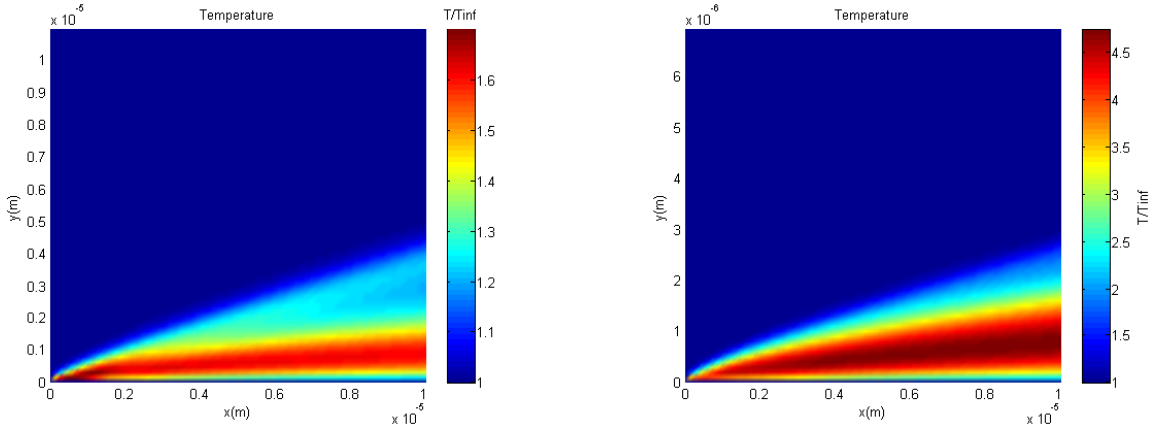

(a) (b)

Figure 4.10. Temperature Contours for Kn=0.009 (a) Mach 4, (b) Mach 10.

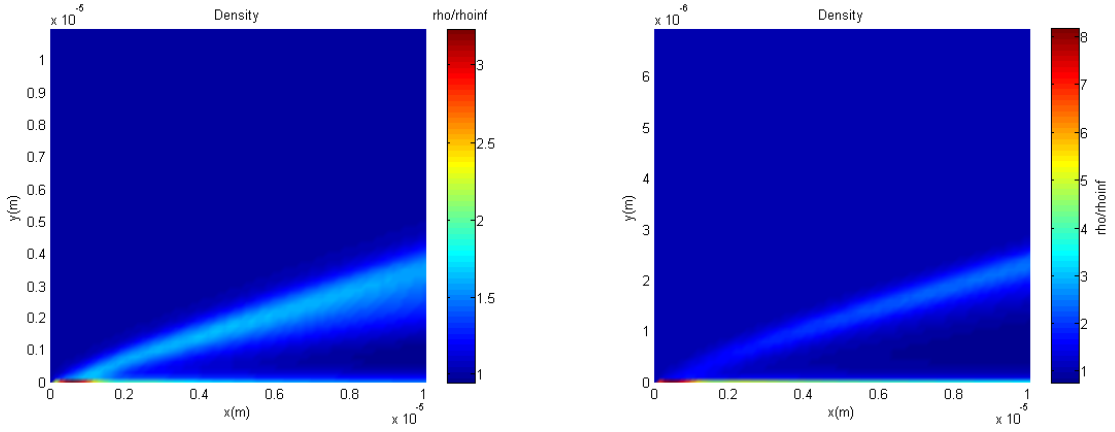

(a) (b)

Figure 4.11. Density Contours for Kn=0.009 (a) Mach 4, (b) Mach 10.

4.4.2 Slip Regime Results

The characteristic length of 1×10^{-5} m is chosen because this length is too small, and it predicts the early occurrence of slip regime. From Figure 4.2, the slip regime occurs at an altitude of 8 km for a characteristic length of 1×10^{-5} m and at an altitude of 57 km for a characteristic length of 1 cm. The corresponding results for 1 cm are plotted in subsequent sections.

Kn=0.0112

At Knudsen number of 0.0112, the slip regime begins to occur in the flow as the free stream atmospheric properties are rarefied. The continuum formulation fails to predict the flow with this Knudsen number. However, the general flow field shows a slighter decrease in the peak value. Figure 4.12(a) shows the pressure contour. Figure 4.12(b) shows the temperature contour. The results in this slip regime is slightly lower than the continuum regime Knudsen number. This is because the molecules slip on the plate surface rather than getting attached to it.

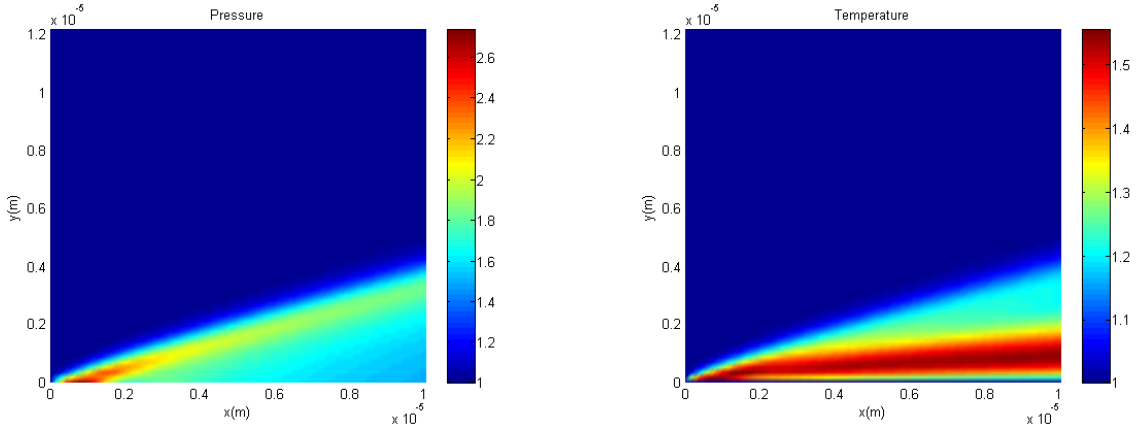

(a) (b)

Figure 4.12. Contour Plots for Kn=0.0112 (a) Pressure, (b) Temperature.

Kn=0.02

At Knudsen number of 0.02, the continuum assumption with slip boundary condition loses its originality as it is a first order slip boundary condition. Use of higher order slip boundary conditions are suggested beyond this Knudsen number. Figure 4.13 shows the pressure and temperature contours. The peak value of the pressure and temperature is lowered with the use of slip conditions. This lower values of the pressure and temperature is because of the slip that is happening at the respective Knudsen number.

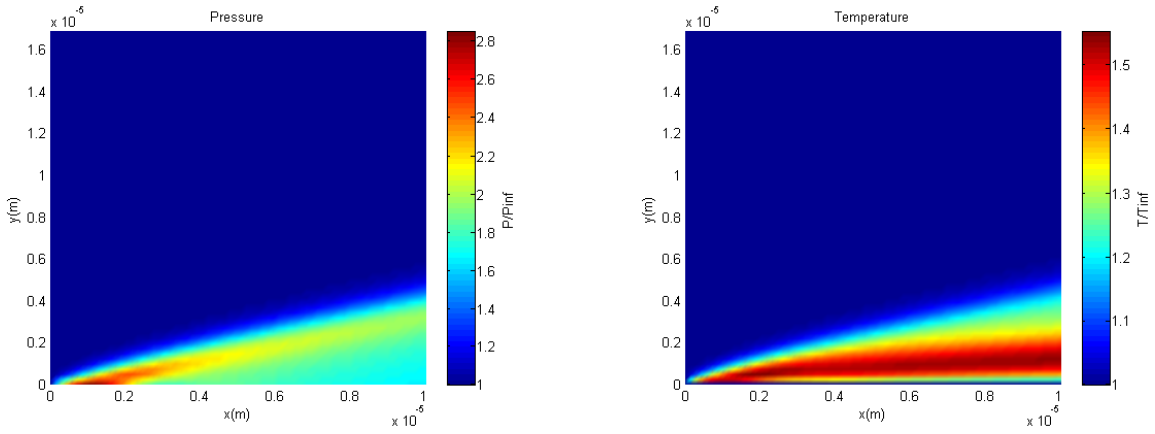

(a) (b)

Figure 4.13. Contour Plots for Kn=0.02 (a) Pressure, (b) Temperature.

As the slip boundary conditions used are of first order, the Navier-Stokes equations will not produce results beyond Knudsen number of 0.02. There are few higher order slip boundary conditions that extends the validity of Navier-Stokes equations till transition regime [60, 61, 62, 63]. The use of such higher order slip boundary conditions is easier when compared to the complex Burnett equations. The overview of the governing equations can be found in Table 3.1.

Before discussing the numerical solutions of the computational model with the solutions from Anderson et al. [3], a few general comments are in order:

1. The steady-state solution for the sea level free stream properties converged after 2050 iterations. The solution is obtained for different grid dimensions to ensure that the model is grid- independent.
2. When plotting the profiles of different flow-field parameters, a normalized y distance, is used. It is given by,

$$\bar{y} = \frac{y}{x}\sqrt{Re_x} \tag{4.4}$$

3. The profiles of various non-dimensional properties are presented.

In Figure 4.14, non-dimensional surface pressure distribution is plotted as a function of length of the plate. Oscillations are apparent in the leading edge region. This is because of the continuum assumption in the locally formed non-equilibrium region or numerical effect. The peak in the trailing edge pressure (Figure 4.14(a)) is because of the strength of the shock wave.

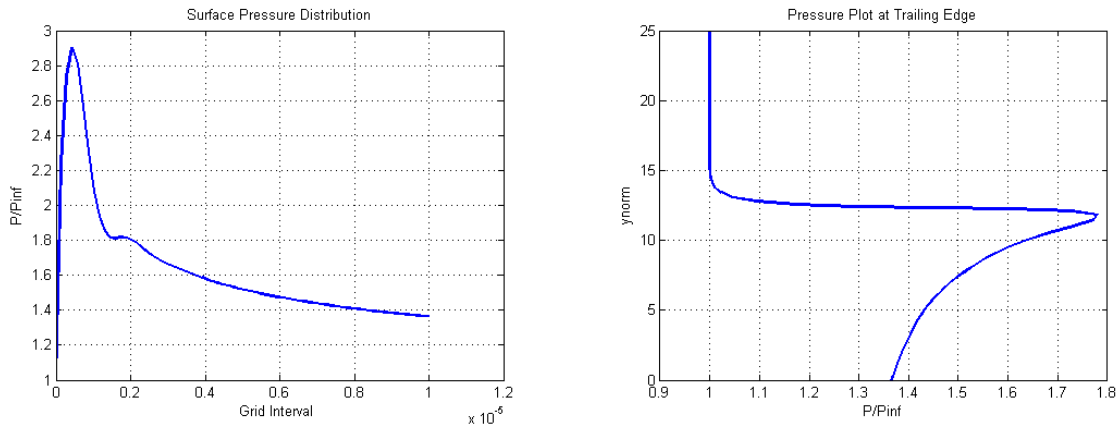

(a) (b)

Figure 4.14. Non-dimensional pressure plots (a) Surface Pressure Distribution, (b) Pressure at trailing edge.

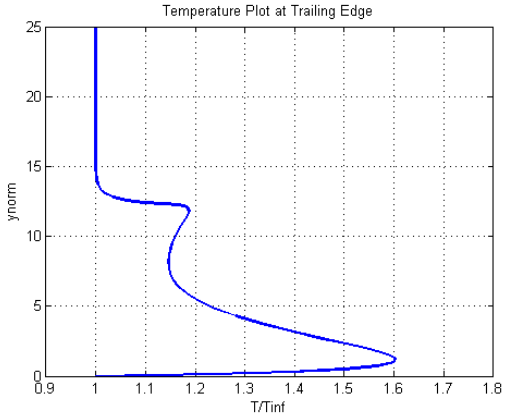

Figure 4.15. Non-dimensional Temperature (at the trailing edge) .

Figure 4.15 shows the temperature plot at the trailing edge. The expanded ordinate of the plot gives clear variation of the parameters in the boundary layer region. As said earlier, the most of the transport mechanism occurs within the boundary layer. This is responsible for this peak value of temperature within the boundary layer. The results from the computational model compares good with the results from the results from Anderson et al. [3].

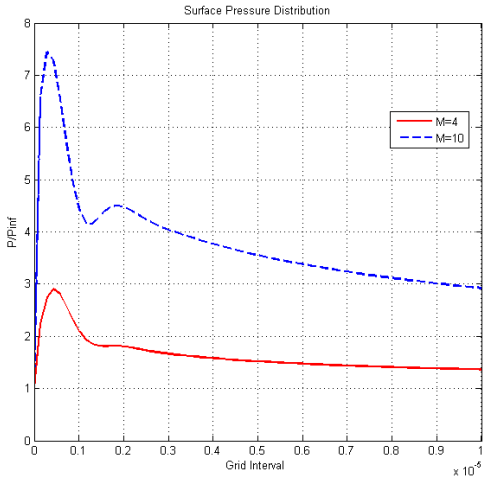

Figure 4.16. Surface Pressure variation for diffferent Mach number .

Figure 4.16 shows the variation in the surface pressure as a function of Mach number for continuum regime at Kn=0.005. The increase in Mach number increases the strength of the shock. This inturn cause the local rarefactions to increase.

Figure 4.17 shows the variation of surface pressure distribution for continuum regimes and slip regimes. When looking at Figure 4.17(b), the oscillations near the tip is widened because of the increase in intensity of the local rarefaction near the tip.

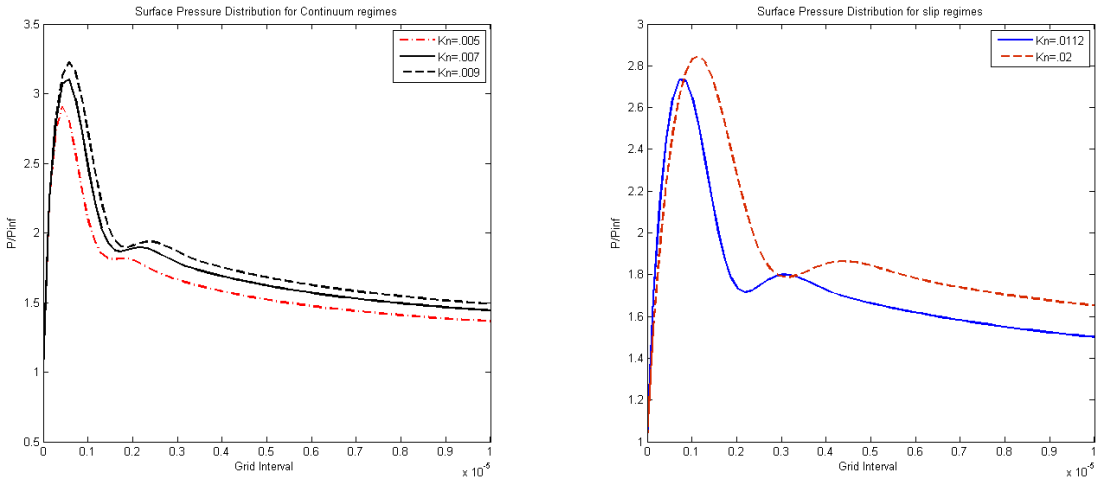

(a) (b)

Figure 4.17. Surface Pressure Variation at M=4 (a) Continuum, (b) Slip.

With increase in altitude, the boundary layer becomes thinner and thinner because of the decrease in density. With higher Mach numbers, the boundary layer gets thinner even more and more aerothermodynamic effects begin to appear. The thinning of the boundary layer is evident from the streamwise velocity plot with nondimensional y distance (Figure 4.18).

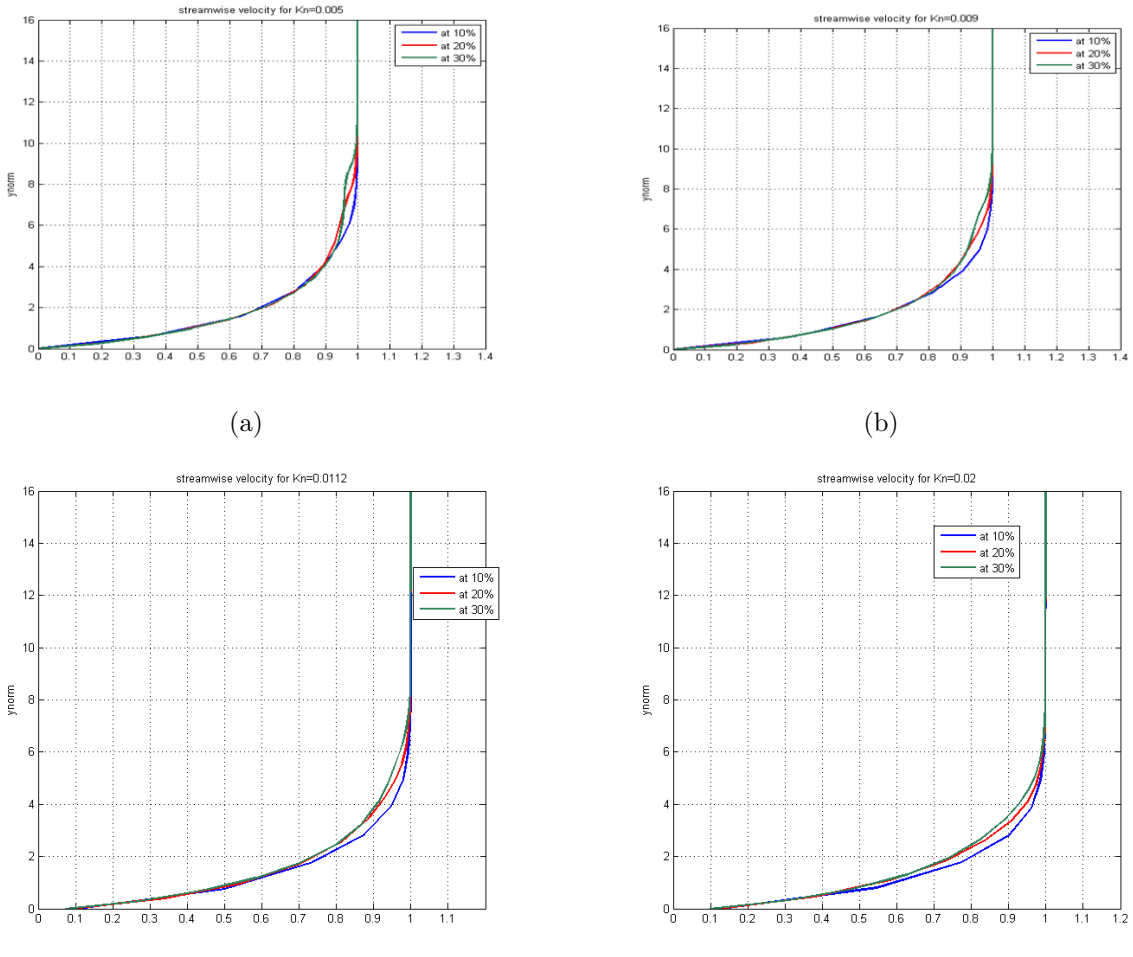

Figure 4.18. Stream wise velocity at M=4 (a) Kn=0.005, (b) Kn=0.009, (c) Kn=0.0112, (d) Kn=0.02.

CHAPTER 5

CONCLUSION AND FUTURE WORK

The computational model developed in the thesis is used to predict the aerothermodynamic flowfield variation over small-scale satellites for earth entry conditions. The inflow free stream properties required by the computational model are P_∞, T_∞, ρ_∞ and V_∞. The first three parameters are obtained from the Standard Atmosphere 1976, and the last parameter is obtained by numerically simulating the equations governing the re-entry of the body. The other parameters required by the model are the domain specifications.

The computational model is used to used to predict the flowfield variations around femtosats for validation. Aerothermodynamic simulations are performed for two different dimensions of the femtosats. The results demonstrate the validity of the unified model in the continuum and slip regime. For specific Knudsen number, flow predictions were validated against results from the DSMC. The flow results matched within 15% for pressure and temperature.

The input free stream velocity (V_∞) causes the major influence on the steady-state results obtained in this thesis. The major contribution of this model is that it uses the kinetic parameters to calculate the flow regimes and choose the the boundary conditions accordingly. It provides the complete distribution of properties in the near environment of the body. The computational algorithm developed in the thesis is limited to the aerothermodynamic analysis of small-scale satellites provided that the entire flowfield lies within the limit of the slip regime. It can be further extended to transition regime with the use of higher order slip conditions. The model can

be coupled with equations governing the re-entry of the small-scale satellites. This coupling produces the complete property distribution at all trajectory points as long as the Knudsen number is within 0.025 .

BIBLIOBRAPHY

[1] Richard H Pletcher, Dale Arden Anderson, John C Tannehill, et al. *Computational fluid mechanics and heat transfer*. CRC Press, 2012.

[2] Graeme Austin Bird. Molecular gas dynamics. *NASA STI/Recon Technical Report A*, 76:40225, 1976.

[3] John D Anderson et al. *Computational fluid dynamics*, volume 206. McGraw-Hill New York, 1995.

[4] Göran Marklund, Lars Blomberg, L Bylander, and P-A Lindqvist. Astrid 2, a low-budget microsatellite mission for auroral research. In *European Rocket and Balloon Programmes and Related Research*, volume 397, page 387, 1997.

[5] O Norberg, S Barabash, I Sandahl, et al. The microsatellite astrid. In *European rocket and balloon programmes and related research*, volume 370, page 273, 1995.

[6] Llas Johnsson. Munin–a swedish nanosatellite. *Paper IAA-B*, pages 4–0406, 2003.

[7] O Norberg, W Puccio, J Olsen, S Barabash, L Andersson, JD Winningham, U Jonsson, and M Eriksson. Munin: A student nanosatellite for space weather information, microsatellites as research tools. In *Proc. of COSPAR Colloquium on Microsatellites as Research Tools, p352-364, Pergamon*, 1999.

[8] Robert Twiggs. Origin of cubesat, 2008.

[9] David J Barnhart, Tanya Vladimirova, and Martin N Sweeting. Very-small-satellite design for distributed space missions. *Journal of Spacecraft and Rockets*, 44(6):1294–1306, 2007.

[10] David J Barnhart. Very small satellite design for space sensor networks. Technical report, DTIC Document, 2008.

[11] David J. Barnhart, Tanya Vladimirova, Adam M. Baker, and Martin N. Sweeting. A low-cost femtosatellite to enable distributed space missions. *Acta Astronautica*, 64(1112):1123 – 1143, 2009.

[12] David J Barnhart. Very small satellite design for space sensor networks. Proc. Brown University ChipSat Workshop, 2010.

[13] Jesse K McTernan, Sven G Bilén, Robert P Hoyt, Nestor R Voronka, and Mason A Peck. Enabling ultra-small sensor spacecraft for the space environment using small-scale electrodynamic tethers, 2011.

[14] Z Manchester and M Johnson. Kicksat–your personal spacecraft in space! *Kickstarter,[Online]. Available: http://www. kickstarter. com/projects/zacinaction/kicksat-your-personal-spacecraft-in-space*, 2013.

[15] Joseph A Schetz and Rodney DW Bowersox. *Boundary layer analysis*. American Institute of Aeronautics and Aeronautics, 2010.

[16] Justin A Atchison, Zachary R Manchester, and Mason A Peck. Microscale atmospheric re-entry sensors. In *International Planetary Probe Workshop*, 2010.

[17] Allen H Julian and Alfred J Eggers. *A study of the motion and aerodynamic heating of missiles entering the earth's atmosphere at high supersonic speeds*. National Advisory Committee for Aeronautics, 1957.

[18] G Koppenwallner, B Fritsche, and T Lips. Survivability and ground risk potential of screws and bolts of disintegrating spacecraft during uncontrolled re-entry. In *Space Debris*, volume 473, pages 533–539, 2001.

[19] T.V. Poplavskaya and V.N. Vetlutskii. A numerical study of a viscous shock layer on a plate. *Journal of Applied Mechanics and Technical Physics*, 38(2): 250–258, 1997.

[20] Henry T Nagamatsu and Ting-Yi Li. Hypersonic flow near the leading edge of a flat plate. *Physics of Fluids*, 3:140, 1960.

[21] HT Nagamatsu. Hypersonic shock wave-boundary layer interaction and leading edge slip. *ARS Journal*, 30(5):454–462, 1960.

[22] TV Poplavskaya and VN Vetlutskii. A numerical study of a viscous shock layer on a plate. *Journal of applied mechanics and technical physics*, 38(2):250–258, 1997.

[23] Ting-Yi Li. Shock-wave effects on the laminar skin friction of an insulated flat plate at hypersonic speeds. *Journal of the Aeronautical Sciences (Institute of the Aeronautical Sciences)*, 20(5), 2012.

[24] J Clerk Maxwell. On stresses in rarified gases arising from inequalities of temperature. *Philosophical Transactions of the royal society of London*, 170:231–256, 1879.

[25] Errol B Arkilic, Martin A Schmidt, and Kenneth S Breuer. Gaseous slip flow in long microchannels. *Journal of Microelectromechanical Systems*, 6(2):167–178, 1997.

[26] Duncan A Lockerby, Jason M Reese, and Michael A Gallis. Capturing the knudsen layer in continuum-fluid models of nonequilibrium gas flows. *AIAA journal*, 43(6):1391–1393, 2005.

[27] Christopher E Glass and James N Moss. Aerothermodynamic characteristics in the hypersonic continuum-rarefied transitional regime. 2001.

[28] Felix Sharipov. Hypersonic flow of rarefied gas near the brazilian satellite during its reentry into atmosphere. *Brazilian Journal of Physics*, 33(2):398–405, 2003.

[29] Felix Sharipov. Aerothermodynamics of brazilian reusable satellite. In *Fourth Symposium on Aerothermodynamics for Space Vehicles*, volume 487, page 373, 2002.

[30] Christopher J Greenshields and Jason M Reese. Rarefied hypersonic flow simulations using the navier–stokes equations with non-equilibrium boundary conditions. *Progress in Aerospace Sciences*, 52:80–87, 2012.

[31] Gordon N Patterson. *Molecular flow of gases*. Wiley New York, 1956.

[32] M Smoluchowski von Smolan. Ueber wärmeleitung in verdünnten gasen. *Annalen der Physik*, 300(1):101–130, 1898.

[33] Duncan A Lockerby, Jason M Reese, David R Emerson, and Robert W Barber. Velocity boundary condition at solid walls in rarefied gas calculations. *Physical Review E*, 70(1):017303, 2004.

[34] R Co. Boundary condition for fluid flow: curved or rough surfaces. *Physical review letters*, 1990.

[35] I.V Egorov and A.I Erofeev. Continuum and kinetic approaches to the simulation of the hypersonic flow past a flat plate. *Fluid dynamics*, 32(1):112–122, 1997.

[36] US NOAA and US Air Force. Us standard atmosphere, 1976. Technical report, NOAA-S/T, 1976.

[37] Ernst Heinrich Hirschel. *Basics of aerothermodynamics*, volume 206. Springer, 2005.

[38] John D Anderson. *Hypersonic and high temperature gas dynamics*. Aiaa, 2000.

[39] John J Bertin. *Hypersonic aerothermodynamics*. AIAA, 1994.

[40] Walter Guido Vincenti and Charles H Kruger. Introduction to physical gas dynamics. *Introduction to physical gas dynamics, by Vincenti, Walter Guido; Kruger, Charles H. New York, Wiley [1965]*, 1, 1965.

[41] Michael Macrossan. Scaling parameters in rarefied flow:breakdown of navier-stokes equations. Technical Report 2006/03, The University of Queensland, 2006.

[42] Hsue-Shen Tsien. Superaerodynamics, mechanics of rarefied gases. *Journal of the Aeronautical Sciences (Institute of the Aeronautical Sciences)*, 13(12), 2012.

[43] Carlo Cercignani. *The Boltzmann equation*. Springer, 1988.

[44] Sydney Chapman and Thomas George Cowling. *The mathematical theory of non-uniform gases: an account of the kinetic theory of viscosity, thermal conduction and diffusion in gases*. Cambridge university press, 1970.

[45] RT Davis. Numerical solution of the hypersonic viscous shock-layer equations. *AIAA journal*, 8(5):843–851, 1970.

[46] MN Kogan. Molecular gas dynamics. *Annual Review of Fluid Mechanics*, 5(1): 383–404, 1973.

[47] Kazuo Aoki, Kohsuke Kanba, and Shigeru Takata. Numerical analysis of a supersonic rarefied gas flow past a flat plate. *Physics of Fluids*, 9(4):1144–1161, 1997.

[48] SP Popov and FG Tcheremissine. Rarefied gas flow around flat plates. *Journal of Machinery Manufacturing and Automation*.

[49] George Karniadakis, Ali Beskok, and Narayan Aluru. Governing equations and slip models. *Microflows and Nanoflows: Fundamentals and Simulation*, pages 51–77, 2005.

[50] RW MacCormack and H Lomax. Numerical solution of compressible viscous flows. *Annual Review of Fluid Mechanics*, 11(1):289–316, 1979.

[51] Peter Lax and Burton Wendroff. Systems of conservation laws. *Communications on Pure and Applied Mathematics*, 13(2):217–237, 1960. ISSN 1097-0312. doi: 10.1002/cpa.3160130205. URL `http://dx.doi.org/10.1002/cpa.3160130205`.

[52] R MacCormack. Current status of numerical solutions of the navier-stokes equations. 1985.

[53] G Koppenwallner, B Fritsche, and T Lips. Multidisciplinary analysis tools for orbit and reentry. In *Hyperschall Technologie Goettingen, Kallenburg-Lindau, Germany, presented at the 3rd International Workshop on Astrodynamics Tools and Techniques, ESTEC, Noordwijk, Netherlands*, 2006.

[54] Tobias Lips and Bent Fritsche. A comparison of commonly used re-entry analysis tools. *Acta Astronautica*, 57(2):312–323, 2005.

[55] B Fritsche, G Koppenwallner, and M Ivanov. *Advanced Model for Spacecraft Disintegration During Atmospheric Re-Entry*. Hypersonic Technology Gottingen, 2000.

[56] Hrvoje Jasak, Aleksandar Jemcov, and Zeljko Tukovic. Openfoam: A c++ library for complex physics simulations. In *International Workshop on Coupled Methods in Numerical Dynamics, IUC, Dubrovnik, Croatia*, pages 1–20, 2007.

[57] TJ Scanlon, E Roohi, C White, M Darbandi, and JM Reese. An open source, parallel dsmc code for rarefied gas flows in arbitrary geometries. *Computers & Fluids*, 39(10):2078–2089, 2010.

[58] Jeffrey Allen and Thomas Hauser. foamdsmc: An object oriented parallel dsmc solver for rarefied flow applications. In *45th AIAA Aerospace Sciences Meeting and Exhibit, Reno, Nevada*, 2007.

[59] Zhi-Xin Sun, Zhen Tang, Ya-Ling He, and Wen-Quan Tao. Proper cell dimension and number of particles per cell for dsmc. *Computers & Fluids*, 50(1):1–9, 2011.

[60] Nishanth Dongari and Amit Agrawal. Modeling of navier–stokes equations for high knudsen number gas flows. *International Journal of Heat and Mass Transfer*, 55(15):4352–4358, 2012.

[61] AK Sreekanth. Slip flow through long circular tubes. 1969.

[62] George Karniadakis and Ali Beskok. *Micro flows: fundamentals and simulation*. Springer New York, 2002.

[63] Dai Jie, Xu Diao, Khoo Boo Cheong, and Lam Khin Yong. Navier-stokes simulations of gas flow in micro devices. *Journal of Micromechanics and Microengineering*, 10(3):372, 2000.

BIOGRAPHICAL STATEMENT

Sudharsan Thiruvenkadam was born in Chennai, TamilNadu, in 1989. In 2011, he received his B.S. degree in Aeronautical Engineering from Anna University, India. He joined The University of Texas at Arlington in Fall 2011 to pursue his Master degree in Aerospace Engineering. His research interests include Computational Fluid Dynamics, Aerodynamics, Numerical methods, Design and Drafting. He started his thesis under the supervision of Dr. Ben Harris. He published his research work in 66th Annual Division of Fluid dyanamics meeting organized by American Physics Society.